Gernot Friedrichs, Elke Goos, Joachim Gripp, Hauke Nicken, Jan-Boyke Schönborn, Henrik Vogel and Friedrich Temps

The Products of the Reactions of o-Benzyne with Ethene, Propene, and Acetylene: A Combined Mass Spectrometric and Quantum Chemical Study.

Zeitschrift für Physikalische Chemie (2009) Vol. 223, No. 4-5, pp. 387-407.
Festschrift Heinz Georg Wagner

doi: 10.1524/zpch.2009.6042

Zeitschrift für physikalische Chemie

The Products of the Reactions of *o*-Benzyne with Ethene, Propene, and Acetylene: A Combined Mass Spectrometric and Quantum Chemical Study

Gernot Friedrichs*: Institut für Physikalische Chemie, Christian-Albrechts-Universität zu Kiel, Olshausenstr. 40, 24098 Kiel , Germany

Elke Goos: Institut für Verbrennungstechnik, Deutsches Zentrum für Luft- und Raumfahrt e.V. (DLR), Pfaffenwaldring 38 - 40, 70569 Stuttgart , Germany

Joachim Gripp: Institut für Physikalische Chemie, Christian-Albrechts-Universität zu Kiel, Olshausenstr. 40, 24098 Kiel , Germany

Hauke Nicken: Institut für Physikalische Chemie, Christian-Albrechts-Universität zu Kiel, Olshausenstr. 40, 24098 Kiel , Germany

Jan-Boyke Schönborn: Institut für Physikalische Chemie, Christian-Albrechts-Universität zu Kiel, Olshausenstr. 40, 24098 Kiel , Germany

Henrik Vogel: Institut für Physikalische Chemie, Christian-Albrechts-Universität zu Kiel, Olshausenstr. 40, 24098 Kiel , Germany

Friedrich Temps*: Institut für Physikalische Chemie, Christian-Albrechts-Universität zu Kiel, Olshausenstr. 40, 24098 Kiel , Germany

Keywords: chemical kinetics, benzyne, alkenes, PAH formation

MS-ID: Heft: / ()	friedrichs@phc.uni-kiel.de, temps@phc.uni-kiel.de	September 22, 2011

Abstract

The primary products of the bimolecular reactions of *ortho*-benzyne, *o*-C_6H_4 (1,2-dehydrobenzene), with ethene, propene, and acetylene have been detected by molecular beam mass spectrometry at a combustion relevant temperature of $T = 1475$ K. *o*-Benzyne was produced by flash pyrolysis of phthalic anhydride in the absence and presence of the respective reactant. Potential reaction pathways of the addition reactions were investigated by quantum chemical calculations. Channels with biradical intermediates were found to be energetically more favorable than alternative quasi-concerted [2+1] cycloaddition and concerted H-transfer pathways. Bicyclic benzocyclobutene and benzocyclobutadiene were identified as the main products of the reactions with C_2H_4 and C_2H_2, respectively. At combustion temperatures, however, these cyclic products are likely to undergo sequential ring opening. In the case of propene, the presence of an allylic H atom initiates a favorable *ene*-type reaction sequence yielding the open-chain product allylbenzene. Overall, hydrocarbon reactivity was found to increase in the order C_2H_2, C_2H_4 to C_3H_8. The range of the estimated bimolecular rate constants is comparable to the rate constants of the corresponding phenyl radical reactions and hence point out a potentially important role of *o*-C_6H_4 reactions in flame and soot formation chemistry.

Dedication

Prof. Drs. h.c. Dr. rer. nat. Heinz Georg Wagner to his 80th birthday.

1 Introduction

The interest in the reaction kinetics of *ortho*-benzyne, *o*-C_6H_4, stems from its unique role in high temperature phenyl radical, C_6H_5, chemistry. First of all, phenyl radicals are known as important reactive intermediates in benzene flames [1, 2, 3, 4]. The thermal decomposition of benzene is usually described by the Bauer-Aten mechanism [5], which assumes a thermal decomposition of C_6H_5 according to

$$C_6H_5 + M \rightarrow C_4H_3 + C_2H_2 + M \rightarrow C_4H_2 + C_2H_2 + H + M, \qquad (1)$$

with diacetylene and acetylene as the main ring cleavage products. The probably most important bimolecular reaction of the phenyl radical is its reaction with acetylene yielding phenylacetylene, $C_6H_5C_2H$,

$$C_6H_5 + C_2H_2 \rightarrow C_6H_5C_2H + H \overset{\text{HACA}}{\rightsquigarrow} \text{PAH} \rightsquigarrow \text{soot}. \qquad (2)$$

In this way, a polycyclic aromatic hydrocarbon (PAH) forming H-abstraction C_2H_2-addition (HACA) sequence [6] is initiated that finally results in the formation of soot. However, more recently this traditional description of phenyl radical chemistry has been challenged by the fact that *o*-benzyne, *o*-C_6H_4, has been identified as a thermodynamically favorable main product of the thermal unimolecular decomposition of phenyl [7, 8, 9].

$$C_6H_5 + M \rightarrow o\text{–}C_6H_4 + H + M. \qquad (3)$$

According to statistical rate theory calculations performed by Madden et al.[8], under thermal conditions, the commonly assumed phenyl decyclization process according to equation 1 does not play a role at all. Instead, the experimentally proven diacetylene and acetylene formation was explained by a subsequent thermal decomposition of the *o*–C_6H_4 [10, 11, 12],

$$o\text{–}C_6H_4 + M \rightarrow C_4H_2 + C_2H_2 + M. \qquad (4)$$

In this respect, the primary products of the traditional and revised Bauer-Aten mechanisms are the same. This view is confirmed by a recent extensive study of Zhang et al.[12] on the identification of the reaction products of *o*-C_6H_4 decomposition by means of time-of-flight photoionization mass spectrometry, matrix-isolation Fourier transform infrared absorption spectroscopy, chemical ionization mass spectrometry, and rigorous *ab initio* electronic structure computations. Zhang et al. found that *o*-benzyne cleanly decomposes to the retro-Diels-Alder fragments C_4H_2 and C_2H_2.

The role of an alternative isomerization pathway,

$$o\text{–}C_6H_4 \rightarrow m\text{–}C_6H_4 \rightarrow p\text{–}C_6H_4 \rightarrow HC_2\text{–}C_2H_2\text{–}C_2H, \qquad (5)$$

where the enediyne (Z)-hexa-3-en-1,5-diyne is formed by Bergman fragmentation of the *p*-benzyne isomer, remains unclear. Whereas calculations by Moskaleva et al.[11] predicted this isomerization channel to be significant at temperatures of $T < 2000$ K, the experiments of Zhang et al.[12] indicate the absence of the enediyne product. In another study, Xu et al.[13] investigated the thermal dissociation of *o*-benzyne behind shock waves, where H atoms were detected by means of H atom resonance absorption spectroscopy. According to Xu et al., detected H atoms can be attributed to yet another minor high temperature decomposition channel,

$$o\text{-}C_6H_4 + M \rightarrow C_6H_3 + H + M, \tag{6}$$

and a channel branching fraction of 0.17 at $T = 2000$ K and $p \approx 1.7$ bar was reported.

Only very little is known to date about the products and kinetics of combustion-relevant bimolecular reactions of *o*-benzyne in the gas phase. Similar to the reaction sequence outlined in equation 2, reactions of *o*-C_6H_4 with unsaturated molecules, in particular C_2H_2, may be of substantial importance as potential sources for large PAH in combustion processes, whose formation and destruction pathways are far from being well understood [7, 14, 15]. Additionally, *o*-C_6H_4 is an intriguing reactive molecule in its own right for its key role in nucleophilic aromatic substitution in organic synthesis [16].

o-Benzyne can be produced in gas phase experiments by UV photolysis [17, 18, 19] or pyrolysis [13, 20, 21] of several precursors, for example benzenediazonium-2-carboxylate, phthalic anhydride, 1,2-dibromo- or 1,2-diiodobenzene, or benzoylchloride. Berry and coworkers succeeded to measure the UV absorption spectrum of *o*-C_6H_4 [17]. Subsequently, they and Porter and Steinfeld estimated the rate constant for the dimerization reaction of *o*-C_6H_4 to biphenylene [22, 18]. These early results were discussed in terms of a biradical *o*-benzyne structure. Only after long debates about the observation of different IR spectra, the C≡C stretching vibration of *o*-C_6H_4 was finally assigned to a band at $\tilde{\nu} = 1846$ cm^{-1} [23]. Although this wavenumber is low compared to a value of a normal C≡C stretching vibration (2100-2300 cm^{-1}), *o*-C_6H_4 has to be considered as an alkyne rather than a biradical on the grounds of its sizeable singlet-triplet energy gap (≈ 158 kJ/mol) [24]. Note, however, that the C-C≡C bond angle in *o*-benzyne (127°) is substantially smaller than in the idealized linear geometry for *sp* hybridization. The resulting ring strain induces some biradical character, amounting to about 10% of the ground state singlet electonic wave function [25]. Conclusive information on the structure of *o*-C_6H_4 was eventually provided by high resolution microwave spectra [26, 27, 28].

As expected for a cycloalkyne, *o*-benzyne can undergo [2+4] symmetry-allowed Diels-Alder- and *ene*-type cycloadditions with complete retention of the stereochemistry of the alkene in the adduct [29, 30]. In

contrast, the concerted [2+2] cycloaddition is symmetry-forbidden and the reaction can be assumed to proceed stepwise involving a biradical species and resulting in a loss of stereochemistry. Surprisingly, the production of highly stereospecific cycloadducts was reported for the reaction of cyclopentyne with *cis*- and *trans*-2-butene [31]. The additions of *o*-benzyne to *cis*- and *trans*-1,2-dichloroethene yield products with (moderate) retention of the original stereochemistry as well [32]. Quite recently, Kinal and coworkers [33, 34] and Bachrach and Gilbert [35] resolved the continuing discussion on the nature of the cycloaddition mechanism. Based on *ab initio* calculations they proposed a multistep mechanism passing through a concerted [2+1] transition state and an *edge-on* reaction intermediate (Scheme 1). This pathway, which is in complete agreement with the experimentally observed stereospecificity, competes with the biradical pathway. Moreover, both pathways are interlinked by a transition state structure that connects the *edge-on* carbene and the biradical intermediate.

In this paper, we report on a combined experimental and theoretical investigation of the primary products of the reactions of *o*-C_6H_4 with the prototypical small unsaturated hydrocarbon molecules ethene, propene, and acetylene. Some preliminary experiments were performed on butene as well and will be briefly outlined together with the propene data. *o*-benzyne was produced by pyrolysis of phthalic anhydride in a SiC flash pyrolysis reactor coupled to a molecular beam quadrupole mass spectrometer. The interpretation of the observed mass spectra obtained in presence of the hydrocarbon reactant was complemented by detailed quantum chemical *ab initio* calculations at the DFT and MP2 levels of theory. Taking into account concerted and biradical reaction pathways, which yield both bicyclic and open-chain products (phenyl substituted hydrocarbons), we were able to establish the primary addition products and their subsequent fragmentation routes.

2 Methods

2.1 Experimental Setup

The experimental setup for the study of the products of the *o*-C_6H_4 reactions consisted of a pulsed SiC flash pyrolysis jet reactor based on the design of Chen [36]. A photograph of the assembly is shown in Fig. 1. The jet reactor, which was attached to a removable flange by two copper rods in a first high vacuum chamber, was connected to a molecular beam sampling quadrupole mass spectrometer for the product analysis in a second vacuum chamber. The 60 mm long SiC pyrolysis tube (Saint-Gobain Ceramics, 2.5 mm o.d., 1 mm i.d.) was attached to a solenoid actuated pulsed molecular beam valve (General Valve Series 9) through a Macor spacer. The last 23 mm of the tube were resistively heated to a desired temperature in the range between 1080 and 1620 K by an electrical circuit

with two commercial halogen radiators in series compensating for the decrease of the resistance of the SiC with increasing temperature. With its low heat conductivity, the Macor spacer isolated the SiC tube thermally against the solenoid valve assembly. The phtalic anhydride (PA) used as precursor for the o-C_6H_4 was contained in a 13×15 mm cylindrical glass vessel with a central bore sitting in a heated stainless steel chamber immediately before the body of the solenoid valve. The entire reservoir/valve assembly was heated to 110°C using a brass jacket with surrounding 1.5 mm NiCr thermocoax wire. The temperature of the jacket was regulated using a Pt100 sensor. Argon carrier gas and gaseous reactants were added through a 6 mm stainless steel tube.

Experiments were run in a pulsed mode, where the solenoid valve was operated at typically 1 Hz repetition rate with opening times of approximately 1 ms. The resulting gas pulses containing the PA precursor and the reactant gases passed through the SiC flash pyrolysis reactor before expanding into the vacuum chamber in a free jet. A small amount of the gas mixtures with the reaction products was extracted in a molecular beam formed by a 0.5 mm i.d. conical skimmer (Macor ceramics) entering into an Extrel C50 quadrupole mass spectrometer for analysis of the reaction products. Molecular ions formed by low energy electron impact ionization (Bruker MM1) were extracted at right angles, mass filtered in the quadrupole analyzer, and monitored using a channeltron detector. The detector was connected via a preamplifier (Stanford Research SR445) and discriminator to a transient recorder (Spectrum PAD280A) PC card for single ion counting and averaging. The data acquisition was controlled by LabView software. The ionization energy of the mass spectrometer was set to 12 eV to provide a satisfactory signal-to-noise ratio at a still acceptable low fragmentation rate of the molecular ions. Mass spectra of the reaction mixtures were recorded by accumulating the ion signals at a selected m/z value for 10 – 25 gas pulses before switching to the next m/z. The setup had the advantage of allowing us to simultaneously monitor the o-benzyne reaction products in the gas pulses leaving the SiC flash pyrolysis reactor and the background count rates before and after the gas pulses, thereby enabling us to determine even very weak product peaks at a selected m/z value with sufficient contrast ratio.

The temperature of the SiC pyrolysis tube in the experiments was determined using two independent methods. Routine measurements were carried out with a calibrated pyrometer (Keller HCW). A “grey body” correction (factor 0.9) was performed to allow for the deviation of the emission spectrum of SiC from a black body. The resulting pyrometer data were periodically checked using a kinetic calibration method based on the unimolecular decomposition of allylethylether (allylethylether → propene + acetaldehyde) devised by Zhang et al.[20]. Here, the kinetic temperature was extracted from temperature dependent product yields assuming a simple first-order decomposition kinetics. Both methods were found to agree well within $\Delta T \approx \pm 25$ K. Based on the known Arrhe-

nius parameters of the allylethylether decomposition [37, 38], the same measurements were used to estimate an effective reaction time t_{eff} of the reaction mixture in the SiC tube. A reasonable value of $t_{\text{eff}} \approx 65\mu$s was obtained, which is somewhat longer than the minimum conceivable passage time calculated from the sonic speed of Ar, $t_{\text{min}} \approx 39$ μs. A similar calibration method was used to estimate the effective kinetic pressure p_{eff} as well. Briefly, relying upon $t_{\text{eff}} \approx 65\mu$s, unimolecular decomposition rate constants were obtained from measured fractions of thermally decomposed allyliodide, $C_3H_5I \rightarrow C_3H_5 + I$, at different temperatures. An activation energy $E_{\text{a}} = 75$ kJ/mol was extracted from the data. This is significantly lower than the C-I bond dissociation energy ($E_0 = 178$ kJ/mol) and also lower than the activation energy $E_{\text{a}} = 173$ kJ/mol reported by Maloney et al.[39] based on shock tube measurements performed at temperatures $T = 742 - 1068$ K and total pressures around $p \approx 1$ bar. Obviously, our low E_{a} value indicates that the unimolecular allyliodide decomposition took place in the fall-off range under our experimental conditions. Therefore, we calculated approximate fall-off curves based on formalisms outlined by Troe and coworkers [40, 41, 42, 43] with input parameters for vibrational frequencies, rotational constants, and energies taken from MP2/3-21G *ab initio* calculations and thermodynamic data, respectively. First, the experimental data of Maloney et al. were reproduced by fitting the theoretical model. On the one hand, in order to roughly account for the *loose* structure of the activated complex associated with a bond-fission reaction, the high pressure limiting rate constant was scaled by lowering the two vibrational frequencies corresponding to the hindered rotor motion of the allyl fragments. On the other hand, weak collision effects were taken into account by calculating collision efficiencies using an averaged energy transfer parameter $\langle \Delta E_{\text{all}} \rangle = 150$ cm^{-1}. Based on these fall-off curves, we found agreement with our allyliodide rate constant data assuming an experimental pressure of $p \approx 5$ mbar. Finally, taking into account a varied pulsed molecular beam valve backing pressure in the experiments on *o*-benzyne (0.5 bar instead of 1.5 bar), a value of $p_{\text{eff}} \approx 1.7$ mbar was obtained. Note, however, that this estimation relies on many assumptions such that reactant concentrations calculated from p_{eff} are probably not better than a factor of 3 to 5.

Argon as carrier gas (99.999%, Messer Griesheim), the gaseous reactants C_2H_4, C_3H_6, and C_2H_2 (Air Liquide or Messer Griesheim, $\geq 99.6\%$), *trans*-C_4H_8 (Baker), and PA (phtalic anhydride, Merck, $> 99.5\%$) were used as supplied. The gas flows were regulated with calibrated mass flow controllers (Aera). A total gas flow of 5.5 sccm (standard cm^3) was slowly pumped through the precursor chamber allowing the PA vapor pressure to equilibrate. At the precursor reservoir temperature of 387 K used, the PA has a sublimation vapor pressure of 1.43 mbar [44] corresponding to a 0.29 vol-% mixture of phthalic anhydride in Argon. Mass spectra of the reaction mixtures were collected for a pyrolysis temperature of $T \approx 1475$ K using mixing ratios of the reactants of 0.0, 2.5, 5.0, 7.5, and 10 vol-%.

2.2 Quantum chemical calculations

Quantum chemical calculations were carried out to elucidate the main reaction pathways using the Gaussian03 suite of programs [45]. The reactions were explored at the DFT B3LYP/6-311+G(d,p) level and, in the majority of cases, at the MP2/6-311+G(d,p) level of theory as well. Good agreement was found between DFT and MP2 results for calculated relative energies of intermediate and transition state structures. On average, the difference between DFT and MP2 energies was 14 kJ/mol. Start configurations for initial bimolecular reaction steps were selected by "educated guesses". The various transition states were located using the synchronous transit-guided quasi-Newton (STQN, QST2/3), "coordinate-driving", "eigenvector following", and intrinsic reaction coordinate (IRC) methods implemented in Gaussian03. Adding polarization functions on hydrogen atoms was found to be important for the convergence of several H atom transfer transition state structures. The stationary points (minima on the potential energy hypersurface) and transition states were verified by vibrational frequency calculations. "Singlet" biradical structures were calculated using unrestricted wave functions forced by mixing HOMO and LUMO so as to destroy α-β and spatial symmetries (guess=mix keyword in Gaussian03). Spin contaminations were checked by evaluating the expectation value of the $\mathbf{S^2}$ operator. Before annihilation of the first spin contaminant, they were found to be nearly one indicating a mixture of singlet and triplet character. After annhilation, expectation values were lower than 0.1. Due to the small energetic difference between the singlet and triplet state, higher level calculations with configuration interaction (CI) and complete-active-space-self-consistent-field approach (CASSCF) would have been necessary to gain insight into the electron correlation effects and the real electronic nature of the biradical structures.

For the *o*-benzyne + C_2H_4 reaction, Kinal and Piecuch have already performed calculations similar to those reported here [34]. They also considered a possible involvement of triplet state species. The triplet minima of the biradical structures were found to be nearly isoenergetic to the corresponding singlets, apart from that the triplet surface was energetically higher than the singlet surface. As possible significant contribution of reaction pathways following an intersystem crossing step are unlikely, we assumed that all reactions proceed solely on the singlet surfaces. Tables of the energies and structures of the reactants, transition states, intermediates, and products can be requested from the corresponding author.

3 Results

Figures 2a-d show observed mass spectra from the pyrolysis of PA (phtalic anhydride, $C_8H_4O_3$) in Ar at four temperatures, T = 387, 1056, 1457, and 1617 K. The spectra at T = 387 and 1056 K are virtually identical,

showing that PA pyrolysis has not yet started. The main signals are the molecular PA mass peak at m/z = 148 Dalton (PA) and its C_6H_5CO fragment at $m/z = 104$ Dalton. Only a very small signal is seen at the mass of *o*-C_6H_4 ($m/z = 76$) owing to fragmentation of the PA parent ion in the ion source. At T = 1457 K, in contrast, the PA and C_6H_4CO peaks at $m/z = 148$ and 104 Dalton have almost disappeared, but a strong signal has appeared at the mass of $m/z = 76$ Dalton indicating a clean production of *o*-C_6H_4 according to

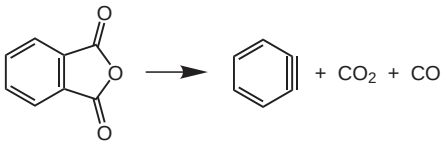

(7)

In addition, signals appear at $m/z = 26$ Dalton (C_2H_2) and 50 Dalton (C_4H_2), which are fragments of *o*-C_6H_4, and at $m/z = 152$ Dalton, which corresponds to biphenylene ($C_{12}H_8$) produced by the dimerization of *o*-C_6H_4,

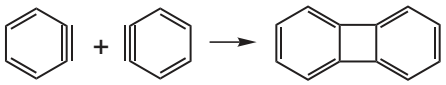

(8)

At $T = 1617$ K, the $m/z = 50$ (C_4H_2) and 26 Dalton (C_2H_2) peaks have increased at the expense of the peaks of the *o*-C_6H_4 and $C_{12}H_8$. In agreement with the findings of Zhang et al.[12], this observation points out a significant unimolecular fragmentation of *o*-C_6H_4 to C_2H_2 and C_4H_2 at $T > 1500$ K. Moreover, we tentatively assign the small peaks at $m/z = 102$ ($C_6H_5C_2H$, phenylacetylene) and 126 Dalton ($C_6H_5C_4H$, phenyldiacetylene) to reaction products of subsequent reactions of acetylene and diacetylene with *o*-benzyne, which will be discussed in more detail in Section 3.3. The origin of the small signal peak at $m/z = 39$ Dalton, which may be indicative for the propargyl radical, C_3H_3, remains unclear.

A plot of the count rates of *o*-C_6H_4 ($m/z = 76$), $C_{12}H_8$ ($m/z = 152$), PA ($m/z = 148$), and the $C_6H_4CO^+$ fragment ($m/z = 104$ Dalton) as function of the pyrolysis nozzle temperature is shown in Fig. 3. Obviously, the (normalized) signals at $m/z = 148$ and 104 Dalton show the same temperature dependencies. The mass signals of *o*-C_6H_4 and $C_{12}H_8$ go through maxima around $T = 1430$ K and $T = 1480$ K, respectively. For the investigation of the products of the title reactions, the pyrolysis temperature was set to $T \approx 1475$ K.

3.1 *o*-Benzyne + ethene

Figure 4 shows mass spectra obtained during studies of the reaction of *o*-C_6H_4 with C_2H_4 at $T = 1473$ K. Panel (a) depicts the spectrum of *o*-C_6H_4

($m/z = 76$ Dalton) and panel (b) the spectrum of C_2H_4 ($m/z = 28$ Dalton) in Ar at the same temperature for comparison. The spectrum of C_2H_4 is identical to that at room temperature, indicating that the thermal decomposition of C_2H_4 can be neglected. Spectrum (c) shows the spectrum obtained for pyrolysis of PA in the presence of ethene. For the sake of clarity, the strong ethene signals around $m/z = 28$ Dalton have been clipped. A new mass signal at $m/z = 104$ Dalton is detected that – as is shown in Fig. 4d – increases almost linearly with the concentration of C_2H_4 in the range studied. This peak is attributed to the cross-recombination product C_8H_8 of the two molecules. In principle, this reaction product can be benzocyclobutene or styrene, i.e.

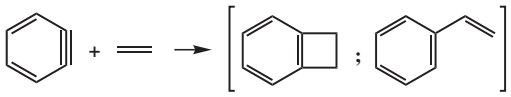

(9)

The detailed reaction pathways were explored using quantum chemistry calculations. Next to the benzocyclobutene forming concerted and biradical pathways outlined in Scheme 1, we identified another concerted pathway forming the open-chain product styrene (Scheme 2). Here, an H atom is directly transferred to the *o*-benzyne ring via a sterically demanding four-membered transition state structure.

Fig. 5 depicts the calculated potential energy diagram for the reaction with zero-point energies stated relative to the sum of the energies of the educts. The following discussion is based on transition state, intermediate, and product energies obtained from our B3LYP/6-311+G(d,p) calculations, which agree very well with literature data reported by Ozkan and Kinal [33]. These authors also performed DFT calculations on the benzocyclobutene forming pathways, but excluded the styrene forming channel. Moreover, B3LYP energies are in good agreement with our MP2/6-311+G(d,p) results as well. First of all, the concerted H-atom transfer pathway forming the open-chain product styrene exhibits the by far highest potential energy barrier (energies connected by short-dashed lines in Fig. 5) and thus can be ruled out to play a significant role for the overall thermal reaction. Most probably, the reaction will take place by surpassing the lowest and, in terms of activation entropy, also less constrained barrier belonging to the biradical pathway instead (solid lines). Subsequently, the biradical intermediate is easily transformed to bicyclic benzocyclobutene by simple rotation and radical recombination of the alkyl radical side chain.

We assume that the formation of this bicyclic product represents the main reaction pathway. Note that a full transition state theory treatment would have been needed (*i*) to accurately quantify relative roles of the biradical versus the "concerted" *edge-on* pathway (long-dashed lines) and (*ii*) to elucidate the role of the isomerization process of the *edge-on* intermediate to the biradical intermediate. However, such a calculation

should be based on higher level *ab initio* potential energy surface data and therefore, in this study, we limit ourselves to a qualitative discussion of the main reaction products based on transition state barrier heights.

3.2 *o*-Benzyne + propene

Mass spectra for the reaction *o*-C_6H_4 with C_3H_6 at $T = 1478$ K are shown in Fig. 6. As before, panel (a) depicts the spectrum of *o*-C_6H_4 (m/z = 76 Dalton), panel (b) that of C_3H_6 ($m/z = 42$ Dalton) in Ar at the same temperature for comparison. Thermal decomposition of C_3H_6 is negligible under the conditions used. The mass spectrum from the pyrolysis of PA in the presence of C_3H_6 is given in panel (c). Apart from a very weak peak at $m/z = 118$ Dalton, the cross-recombination product C_9H_{10}, several other product species can be seen at $m/z = 116$ (C_9H_8), 90 (C_7H_6), 28 (C_2H_4), and 15 Dalton (CH_3). These signals exhibit similar trends with increasing concentrations of C_3H_6 and are attributed to unimolecular decomposition and/or fragmentation of the cross-recombination product ($m/z = 118$ Dalton) in the ion source. Feasible recombination products of the reaction are bicylic 1-methylbenzocyclobutene and several open-chain products including *E*- and *Z*-1-phenylpropene, α-methylstyrene, *o*-methylstyrene, and allylbenzene.

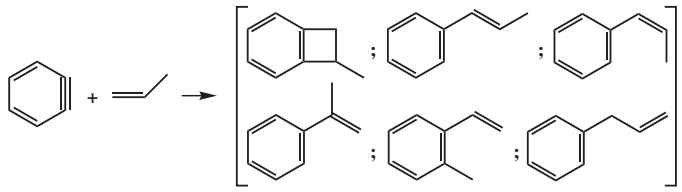

(10)

Additional small signals detected at $m/z = 148$ (PA), 104 (C_6H_4CO), and 65 Dalton (C_5H_5) are independent of the C_3H_6 concentration. The peaks at $m/z = 148$ and 104 Dalton show the same intensity ratio as in the pure PA spectra and are likely due to unpyrolyzed PA, which was deposited on the walls of the vacuum chamber after prolonged experiments. The origin of the weak $m/z = 65$ signal, however, remains unclear.

Quantum chemical calculations reveal that the potential energy diagram for the reaction *o*-C_6H_4 with C_3H_6 (Fig. 7, B3LYP/6-311+G(d,p)) is very similar to that of the ethene reaction. Again, all H-atom transfer pathways, where several transition state structures with different orientations of the methyl substituent exist, are high in energy and do not play a role. For the sake of clarity, only the energetically lowest H-atom transfer pathway forming the *E*-1-phenylpropene with internal double bond in the alkyl substituent is shown in Fig. 7. Exhibiting a transition state energy of 168 kJ/mol, an alternative CH_3 transfer pathway forming *o*-methylstyrene lies far-off in energy and has been omitted in Fig. 7 as well.

The main difference between ethene and propene is, however, the presence of an allylic hydrogen in propene, making possible an *ene*-type cycloaddition reaction according to Scheme 3. This concerted *ene*-reaction pathway passes through a six-membered cyclic transition state with a critical energy of 20 kJ/mol, which is significantly lower than the energy of the first transition state of the biradical pathway (33 kJ/mol). Therefore, we assume the allylbenzene to constitute the main primary reaction product.

Assuming an open-chain product, it should be expected that the parent ion of allylbenzene yields the fragment ions benzyl/tropylium ($m/z = 91$ Dalton, C_7H_7) and vinyl ($m/z = 27$ Dalton, C_2H_3) according to a benzyl fragmentation mechanism. This fragmentation pathway is seen in many alkyl substituted benzenes and is favored due to the formation of the stable tropylium cation, which is in equilibrium with the benzyl cation. Although both the $m/z = 91$ and $m/z = 27$ Dalton peaks are present in the mass spectra shown in Fig. 6c, more pronounced mass signals are seen at $m/z = 90$ and $m/z = 28$ Dalton. An explanation of these signals could be the fast thermal decomposition of allylbenzene according to a retro-carbene CH-insertion, C_6H_5-CH_2-CH=CH_2 → C_6H_5-CH + CH_2=CH_2, yielding directly (singlet) phenylcarbene ($m/z = 90$ Dalton, C_7H_6) and ethene ($m/z = 28$ Dalton). However, at the high pyrolysis temperature used, also other reactions, e.g., the rearrangement of the terminal alkene allylbenzene via a [1,2]-H-shift to the thermodynamically more stable 1-phenylpropene with an internal C=C-double bond, cannot be ruled out. These potential additional reaction products and their fragmentation patterns severely interfere with a complete assignment of the observed mass spectra.

We also performed preliminary experiments on the reaction of *o*-C_6H_4 with *trans*-butene. We failed to detect the mono-addition product at $C_{10}H_{12}$ at $m/z = 132$ Dalton (signal peaks were found at $m/z = 128$, and $m/z = 129$ instead), but obtained strong signals on $m/z = 90$ and $m/z = 28$ Dalton just as well. In case of butene, a clear indication for a secondary reaction comes from an observed mass peak at $m/z = 166$ Dalton ($C_{13}H_{10}$), which we tentatively assign to a thermal reaction product of a species of mass $m/z = 90$ with *o*-benzyne ($m/z = 76$) yielding, e.g., fluorene. Altogether, the butene data seem to fit into the overall picture; however, since no quantum chemical calculations have been performed on this system yet, we will not go further into the details of these experiments.

3.3 *o*-Benzyne + acetylene

Figure 8 shows the observed mass spectra for the reaction of *o*-benzyne with C_2H_2 at $T = 1473$ K. As before, panel (a) depicts the spectrum of *o*-benzyne ($m/z = 76$ Dalton) for comparison. The mass spectrum of C_2H_2 ($m/z = 76$ Dalton) shown in panel (b) is identical to the one at room

temperature, indicating that the thermal decomposition of C_2H_2 can be neglected. The mass spectrum from the pyrolysis of PA in the presence of C_2H_2 is depicted in panel (c). As can be seen, the reaction between *o*-C_6H_4 and C_2H_2 leads to a new mass signal at $m/z = 102$ Dalton. This signal increases linearly with the added acetylene concentration (Fig. 8d) and can be attributed to the cross-recombination products benzocyclobutadiene or phenylacetylene.

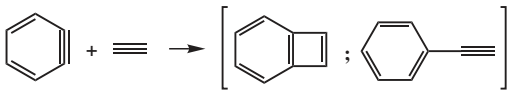

(11)

The results of the B3LYP/6-311+G(d,p) quantum chemical calculations are shown in Fig. 9. As for ethene and propene, the concerted H-atom transfer path forming the open-chain product phenylacetylene exhibits a comparatively high transition state barrier and thus phenylacetylene can be excluded as the primary reaction product. Note, however, that the corresponding transition state structure did not fully converge. Probably due to the flat potential energy surface arising from low-frequency out-of-plane vibrations, the fully optimized transition state was not found and thus its energy is less reliable. Unlike in case of the alkenes, we were not able to clearly differentiate between a biradical and a "concerted" *edge-on* pathway. Instead, an early stage acetylene/*o*-benzyne addition complex with a shallow energy minimum was found. Its structure is similar to the structures of the biradical intermediates found for ethene and propene, nevertheless, this intermediate easily converts to the *edge-on* complex in place of ring-closure. Finally, the ring-closure step of the *edge-on* complex takes place over a relatively high barrier of 63 kJ/mol, indicating the very strained nature of the cyclobutadiene-like transition state. We assume benzocyclobutene to constitute the main primary reaction product. Note, however, that subsequent isomerisation of the ring strained cyclobutadiene is likely, but could neither be excluded nor verified by the measured mass spectra.

4 Discussion

4.1 Reaction pathways

o-Benzyne was shown to be reactive towards unsaturated hydrocarbons (ethene, propene, butene, and acetylene) at combustion temperatures. Bicyclic and open-chain addition products were identified as the main reaction products. Based on quantum chemical calculation, four principally different reaction pathways were identified. The concerted, direct H- (and CH_3-) transfer pathway via four-membered transition states forms open-chain reaction products. It was found to exhibit the highest transition state barriers and probably does not play a role for the overall reactions.

Both the "concerted" pathway, which passes through a [2+1] *edge-on* reaction intermediate, and the biradical pathway give rise to bicyclic reaction products. Accordingly, benzocyclobutene and benzocyclobutadiene are predicted as the main products for the reactions of *o*-benzyne with ethene and acetylene, respectively. As can be concluded from the calculated transition state barriers, the biradical pathways are energetically favored such that the reactivity of *o*-benzyne can be described as (singlet) biradical-like. However, the aryne structure of *o*-benzyne becomes apparent in a pericyclic reaction pathway involving the "triple" bond as well. In this fourth reaction pathway, a concerted, *ene*-type reaction via a six-membered cyclic transition state opens up for reactants with allylic hydrogen atoms. As was shown for propene, this open-chain product forming *ene*-type reaction exhibits the lowest transition state barrier of all four reaction pathways, making it the dominating pathway for larger hydrocarbons like butene.

Sophisticated calculations of the reaction rate constants of bimolecular *o*-benzyne hydrocarbon reactions should be based on more reliable reaction barrier heights obtained from high-level *ab initio* calculations. Appropriate quantum chemical methods such as multireference and perhaps spin-flip coupled-cluster methods with large basis sets are necessary to properly take into account electron correlation and close-lying singlet and triplet states in the discussed biradical pathways.

4.2 Reactivity of *o*-benzyne

Table 1 compares the reactivity of *o*-benzyne towards the three prototype reactants acetylene, ethene, and propene. For the sake of completeness, preliminary data on *trans*-butene are included as well. The second column of Table 1 specifies the relative depletion of the *o*-benzyne concentration measured by monitoring the mass signal at $m/z = 76$ Dalton with and without the addition of 10 vol-% hydrocarbon to the reactant mixture at a temperature of $T \approx 1475$ K. Whereas the scarcely detectable decrease of the signal in case of acetylene (ratio = 0.98) indicates a low reactivity of C_2H_2, an increasingly significant depletion of *o*-benzyne in the order of ethene (0.83), propene (0.72), and *trans*-butene (0.35) is evident. This trend in reactivity is in qualitative agreement with the calculated transition state barriers of the energetically lowest reaction pathways obtained from the quantum chemical calculations (third column), where the assumed reaction products are given in the fourth column of Table 1.

Knowing the *effective* reaction time and pressure of the reacting mixture in the heated SiC tube from the calibration experiments outlined in the Experimental Section, it is possible to estimate the overall bimolecular rate constants. Assuming that the *o*-benzyne depletion is dominated by the reactions *o*-C_6H_4 + alkenes/acetylene, a simple pseudo-first order treatment (0.29 vol-% *o*-benzyne $\ll$ 10% alkenes/acetylene) yields the rate constant values specified in the fifth column of Table 1. Due to the large

uncertainty associated with the absolute concentrations of the reactants, these numbers are probably accurate to merely a factor of 5, however, they are useful as a first rough estimate for the high temperature rate constants of these reactions. A quick consistency check of the obtained values can be performed by assuming a simple Arrhenius temperature dependence of the reaction rate constants. Setting equal the transition state barriers with the respective activation energies, reasonable preexponential factors of $A = \ 1.8 - 7.0 \times 10^{13}$ $cm^3mol^{-1}s^{-1}$ (sixth column in Table 1) were obtained.

Finally, the rate constant value for the reaction *o*-C_6H_4 + C_2H_2, $k \approx 2.2\times 10^{11}$ $cm^3mol^{-1}s^{-1}$, can be compared with the rate constant of the corresponding phenyl radical reaction C_6H_5 + C_2H_2. As already outlined in the introduction, this reaction initiates the HACA sequence that finally results in the formation of soot. According to the revised Bauer-Aten mechanism, however, a large fraction of phenyl radicals decompose to *o*-benzyne such that bimolecular *o*-benzyne reactions might become important as well. With a rate constant value of $k(C_6H_5 + C_2H_2) = 1\times 10^{12}$ $cm^3mol^{-1}s^{-1}$ at $T = 1475$ K, as it is deduced from experimental literature data [46, 47], the phenyl reaction is faster than the *o*-benzyne reaction. Nevertheless, taking into account the large uncertainty of our estimated rate constant and, moreover, the comparatively higher stability of *o*-benzyne in terms of thermal decomposition [8, 11, 9, 13], our experiments point to a potentially important role of *o*-benzyne reactions for the formation of PAH. Overall rate constants found for the reactions of phenyl with C_2H_4, 6.7×10^{11} $cm^3mol^{-1}s^{-1}$ [48], and C_3H_6, 2.2×10^{12} $cm^3mol^{-1}s^{-1}$ [49], ($T = 1475$ K) are of the same order of magnitude as the corresponding *o*-C_6H_4 reactions as well. Clearly, more detailed mechanistic studies and rate constant determinations are needed to clarify the role of *o*-benzyne reactions in flame chemistry and soot formation.

Acknowledgment

We would like to thank Christian Rensing and Carsten Fehling for preliminary studies of the pyrolysis setup during an undergraduate research internship in the group, and Armagan Kinal for help with the DFT treatment of biradical species. The financial support of the work by the Deutsche Forschungsgemeinschaft and Fonds der Chemischen Industrie is gratefully acknowledged.

References

[1] J. D. Bittner and J. B. Howard, Proc. Combust. Inst. **18** (1981) 1105–1116.

[2] J. H. Kiefer, L. J. Mizerka, M. R. Patel, and H. C. Wei, J. Phys. Chem. **89** (1985) 2013–2019.

[3] F. Defoeux, V. Dias, C. Renard, P. J. Van Tiggelen, and J. Vandooren, Proc. Combust. Inst. **30** (2005) 1407–1415.

[4] B. Yang, Y. Li, L. Wei, C. Huang, J. Wang, Z. Tian, R. Yang, L. Sheng, Y. Zhang, and F. Qi, Proc. Combust. Inst. **31** (2007) 555–563.

[5] S. H. Bauer and C. F. Aten, J. Chem. Phys. **39** (1963) 1253–1260.

[6] M. Frenklach, D. W. Clary, W. C. Gardiner Jr., and S. E. Stein, Proc. Combust. Inst. **20** (1985) 887–901.

[7] H. Wang and M. Frenklach, J. Phys. Chem. **98** (1994) 11465–11489.

[8] L. K. Madden, L. V. Moskaleva, S. Kristyan, and M. C. Lin, J. Phys. Chem. A **101** (1997) 6790–6797.

[9] H. Wang, A. Laskin, N. W. Moriarty, and M. Frenklach, Proc. Combust. Inst. **28** (2000) 1545–1555.

[10] W.-Q. Deng, H. K.-L., J.-P. Zhan, and G. He, Chem. Phys. Lett. **288** (1998) 33–36.

[11] L. V. Moskaleva, L. K. Madden, and M. C. Lin, Phys. Chem. Chem. Phys. **1** (1999) 3967–3972.

[12] X. Zhang, A. T. Maccarone, M. R. Nimlos, S. Kato, V. M. Bierbaum, G. B. Ellison, B. Ruscic, A. C. Simmonett, W. D. Allen, and H. F. Schaefer III, J. Chem. Phys. **126** (2007) 44312/1–20.

[13] C. Xu, M. Braun-Unkhoff, C. Naumann, and P. Frank, Proc. Combust. Inst. **31** (2007) 231–239.

[14] H. Wang and M. Frenklach, Combust. Flame **110** (1997) 173–221.

[15] H. Richter, T. G. Benish, O. A. Mazyar, W. H. Green, and J. B. Howard, Proc. Combust. Inst. **28** (2000) 2609–2618.

[16] H. H. Wenk, M. Winkler, and W. Sander, Angew. Chem. Int. Ed. Engl. **42** (2003) 502–527.

[17] R. S. Berry, G. N. Spokes, and M. Stiles, J. Am. Chem. Soc. **84** (1962) 3570–3571.

[18] G. Porter and J. I. Steinfeld, J. Chem. Soc. A **4** (1968) 877–878.

[19] E. W.-G. Diau, J. Casanova, J. D. Roberts, and A. H. Zewail, Proc. Natl. Acad. Sci. USA **97** (2000) 1376–1379.

[20] X. Zhang, A. V. Friderichsen, S. Nandi, G. B. Ellison, D. E. David, J. T. McKinnon, T. G. Lindeman, M. R. Dayton, and M. R. Nimlos, Rev. Sci. Instr. **74** (2003) 3077–3086.

[21] H. Vogel, *Massenspektrometrische Untersuchungen von Reaktionen des* o-*Benzyns mit ungesättigten Kohlenwasserstoffen*, Diploma thesis, Universität Kiel, Germany, 2006.

[22] M. E. Schafer and R. S. Berry, J. Am. Chem. Soc. **87** (1965) 4497–4501.

[23] J. G. Radziszewski, B. A. J. Hess, and R. Zahradnik, J. Am. Chem. Soc. **114** (1992) 52–57.

[24] D. G. Leopold, A. E. S. Miller, and W. C. Lineberger, J. Am. Chem. Soc. **108** (1986) 1379–1384.

[25] A. C. Scheiner, H. F. Schaefer III, and B. Liu, J. Am. Chem. Soc **111** (1989) 3118–3124.

[26] R. D. Brown, P. D. Godfrey, and M. Rodler, J. Am. Chem. Soc. **108** (1986) 1296–1297.

[27] S. G. Kukolich, C. Tanjaroon, M. C. McCarthy, and P. Thaddeus, J. Chem. Phys. **119** (2003) 4353–4359.

[28] E. G. Robertson, P. D. Godfrey, and D. McNaughton, J. Molec. Spectrosc. **217** (2003) 123–126.

[29] R. W. Hoffmann, *Dehydrobenzene and Cycloalkynes*, Academic Press, New York, 1967.

[30] D. M. Hayes and R. Hoffmann, J. Phys. Chem. **76** (1972) 656–663.

[31] L. Fitjer and S. Modaressi, Tetrahedron Lett. **24** (1983) 5495–5498.

[32] M. Jones Jr. and R. H. Levin, J. Am. Chem. Soc. **91** (1969) 6411–6415.

[33] I. Ozkan and A. Kinal, J. Org. Chem. **69** (2004) 5390–5394.

[34] A. Kinal and P. Piecuch, J. Phys. Chem. A **110** (2006) 367–378.

[35] S. M. Bachrach and J. C. Gilbert, J. Org. Chem. **69** (2004) 6357–6364.

[36] D. W. Kohn, H. Clauberg, and P. Chen, Rev. Sci. Instrum. **63** (1992) 4003–4005.

[37] H. Kwart, J. Slutsky, and S. F. Sarner, J. Am. Chem. Soc. **95** (1973) 5242–5245.

[38] K. W. Egger and P. Vitins, Int. J. Chem. Kinet. **6** (1974) 429.

[39] K. L. Maloney, H. B. Palmer, and D. J. Seery, Int. J. Chem. Kinet. **4** (1972) 87–102.

[40] J. Troe, J. Chem. Phys. **66** (1977) 4758–4775.

[41] J. Troe, J. Phys. Chem. **83** (1979) 114–126.

[42] J. Troe, Ber. Bunsenges. Phys. Chem. **87** (1983) 161–169.

[43] R. G. Gilbert, K. Luther, and J. Troe, Ber. Bunsenges. Phys. Chem. **87** (1983) 169–177.

[44] D. Das, S. R. Dharwadkar, and S. R. Chandrasekharaiah, Thermochim. Act. **30** (1979) 371–376.

[45] M. J. Frisch, G. W. Trucks, H. B. Schlegel, G. E. Scuseria, M. A. Robb, J. R. Cheeseman, J. A. Montgomery, Jr., T. Vreven, K. N. Kudin, J. C. Burant, J. M. Millam, S. S. Iyengar, J. Tomasi, V. Barone, B. Mennucci, M. Cossi, G. Scalmani, N. Rega, G. A. Petersson, H. Nakatsuji, M. Hada, M. Ehara, K. Toyota, R. Fukuda, J. Hasegawa, M. Ishida, T. Nakajima, Y. Honda, O. Kitao, H. Nakai, M. Klene, X. Li, J. E. Knox, H. P. Hratchian, J. B. Cross, V. Bakken, C. Adamo, J. Jaramillo, R. Gomperts, R. E. Stratmann, O. Yazyev, A. J. Austin, R. Cammi, C. Pomelli, J. W. Ochterski,

P. Y. Ayala, K. Morokuma, G. A. Voth, P. Salvador, J. J. Dannenberg, V. G. Zakrzewski, S. Dapprich, A. D. Daniels, M. C. Strain, O. Farkas, D. K. Malick, A. D. Rabuck, K. Raghavachari, J. B. Foresman, J. V. Ortiz, Q. Cui, A. G. Baboul, S. Clifford, J. Cioslowski, B. B. Stefanov, G. Liu, A. Liashenko, P. Piskorz, I. Komaromi, R. L. Martin, D. J. Fox, T. Keith, M. A. Al-Laham, C. Y. Peng, A. Nanayakkara, M. Challacombe, P. M. W. Gill, B. Johnson, W. Chen, M. W. Wong, C. Gonzalez, and J. A. Pople, *Gaussian 03, Revision D.01*, Gaussian, Inc., Wallingford, CT, 2004.

[46] A. Fahr and S. E. Stein, Proc. Combust. Inst. **22** (1989) 1023–1029.

[47] E. Heckmann, H. Hippler, and J. Troe, Proc. Combust. Inst. **26** (1996) 543–550.

[48] I. V. Tokmakov and M. C. Lin, J. Phys. Chem. A **108** (2004) 9697–9714.

[49] J. Park, J. Nam, I. V. Tokmakov, and M. C. Lin, J. Phys. Chem. A **110** (2006) 8729–8735.

FIGURES

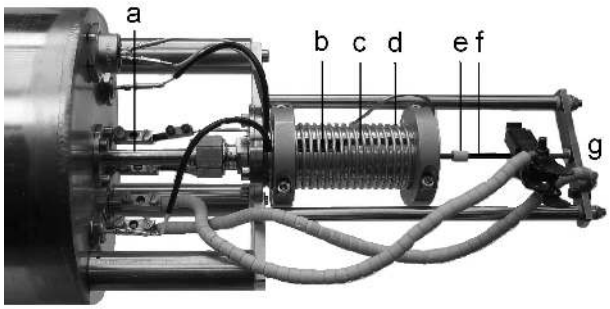

Figure 1: Pulsed SiC flash pyrolysis setup. a: Gas inlet/outlet, b: precursor reservoir, c: pulsed valve, d: heating wire, e: Macor spacer, f: SiC tube, g: gas expansion.

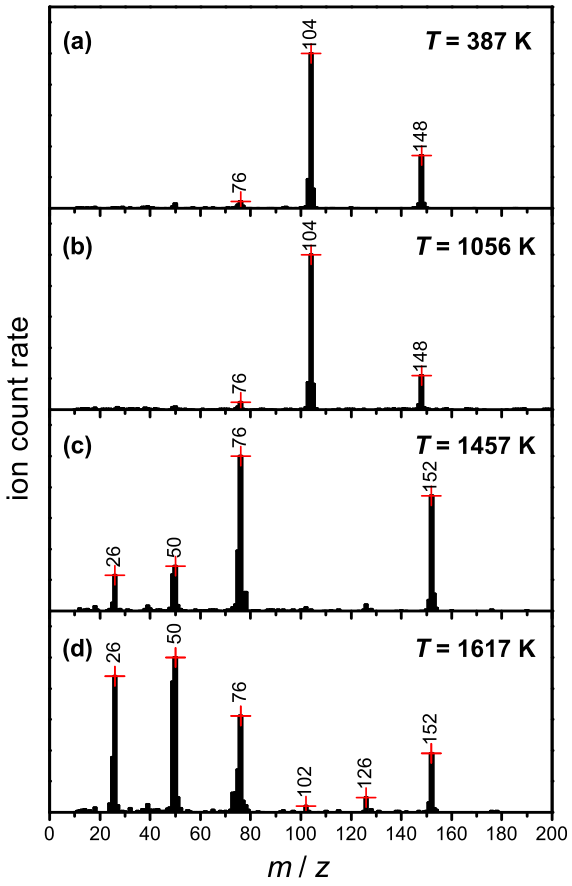

Figure 2: Experimental mass spectra of phthalic anhydride (PA) pyrolysis at different temperatures.

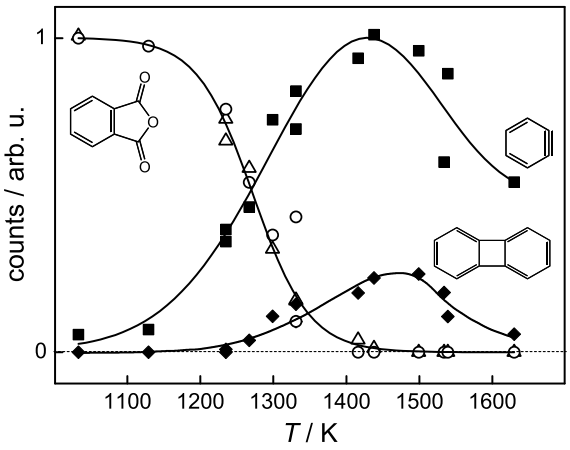

Figure 3: Phthalic anhydride (PA) pyrolysis products. △: PA^+ (m/z = 148 Dalton), ○: $C_6H_5CO^+$ (104 Dalton), ■: o-C_6H_4 (76 Dalton), ♦: $C_{12}H_8$ (152 Dalton).

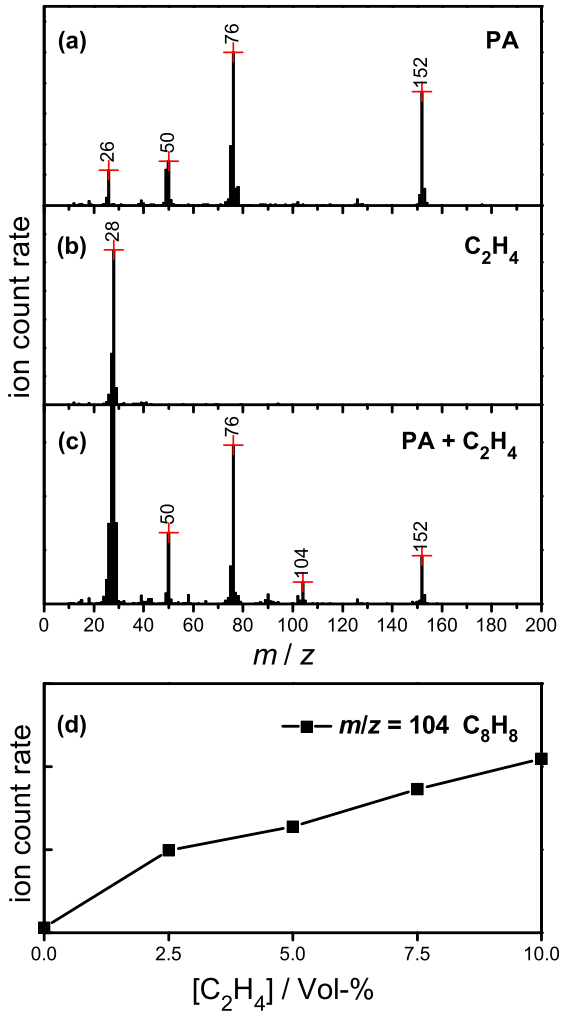

Figure 4: Mass spectra for the reaction *o*-C_6H_4 + C_2H_4 (co-pyrolysis of PA with C_2H_4) at a pyrolysis temperature of T = 1473 K: (a) *o*-C_6H_4, (b) C_2H_4, (c) *o*-C_6H_4 + C_2H_4 (5 vol-%). (d) Mass signal of the reaction product (m/z = 104 Dalton, benzocyclobutene) as function of [C_2H_4].

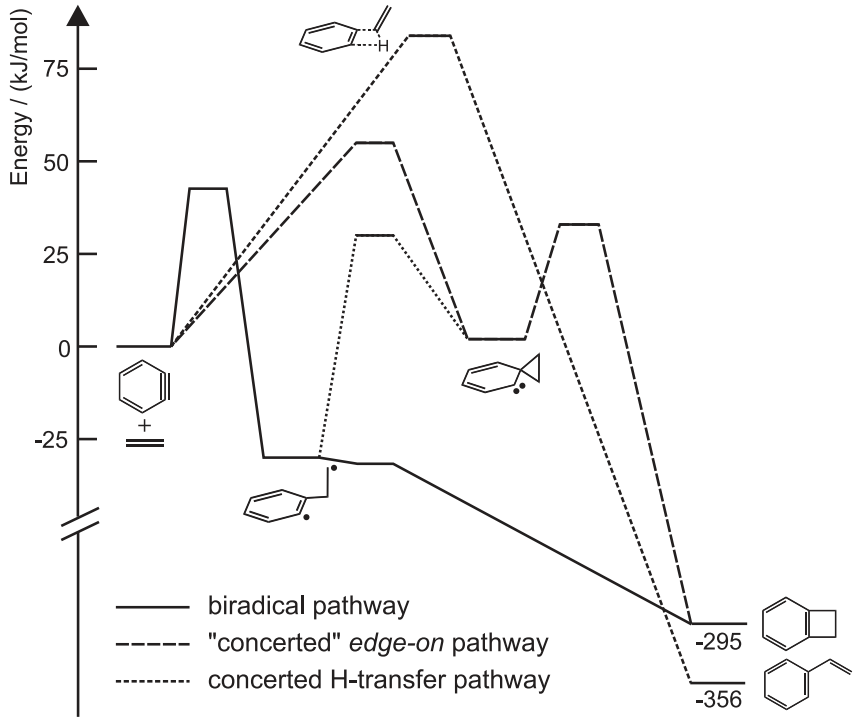

Figure 5: Potential energy diagram for the reaction *o*-C_6H_4 + C_2H_4 as obtained from B3LYP/6-311+G(d,p) calculations. Tables of the energies and structures of all species can be requested from the corresponding author.

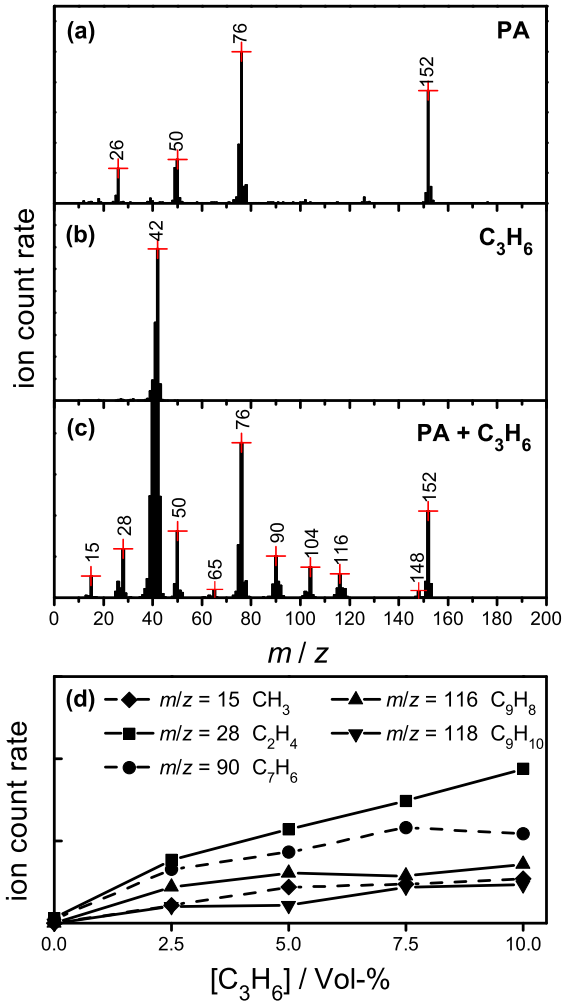

Figure 6: Mass spectra for the reaction *o*-C_6H_4 + C_3H_6 (co-pyrolysis of PA with C_3H_6) at a pyrolysis temperature of $T = 1478$ K: (a) *o*-C_6H_4, (b) C_3H_6, (c) *o*-C_6H_4 + C_2H_4 (5 vol-%). (d) Mass signal of potential reaction products and their fragments as function of [C_2H_6].

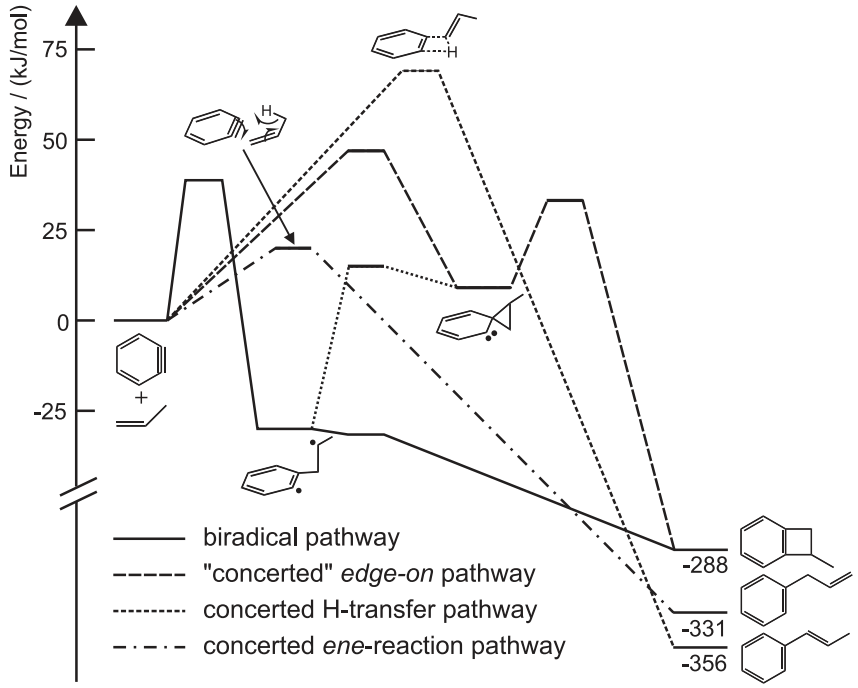

Figure 7: Simplified potential energy diagram for the reaction *o*-C_6H_4 + C_3H_6 as obtained from B3LYP/6-311+G(d,p) calculations. Tables of the energies and structures of all species can be requested from the corresponding author.

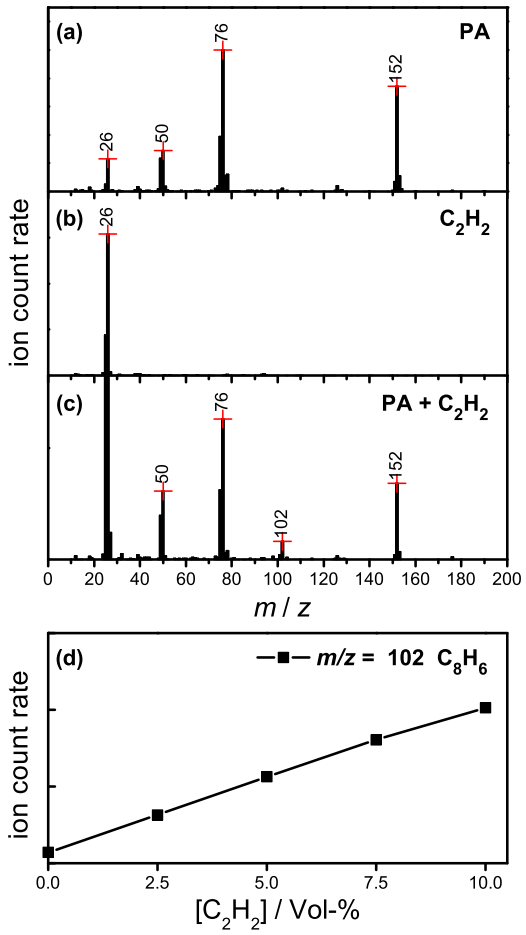

Figure 8: Mass spectra for the reaction *o*-C_6H_4 + C_2H_2 (co-pyrolysis of PA with C_2H_2) at a pyrolysis temperature of T = 1473 K: (a) *o*-C_6H_4, (b) C_2H_2, (c) *o*-C_6H_4 + C_2H_2 (5 vol-%). (d) Mass signal of the reaction product (m/z = 102 Dalton, phenylacetylene) as function of [C_2H_2].

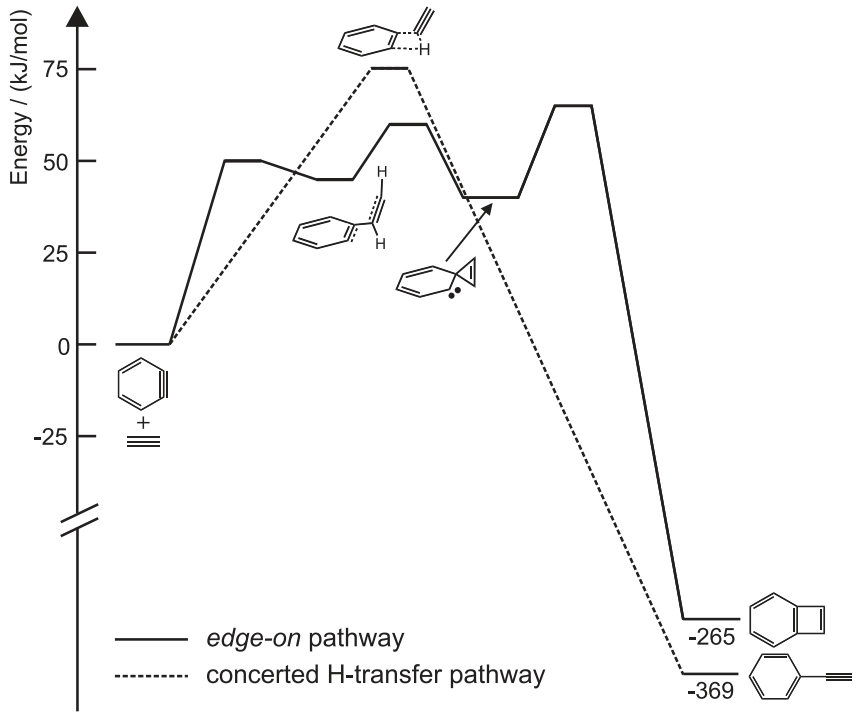

Figure 9: Potential energy diagram for the reaction *o*-C_6H_4 + C_2H_2 as obtained from B3LYP/6-311+G(d,p) calculations. Tables of the energies and structures of all species can be requested from the corresponding author.

SCHEMES and TABLES

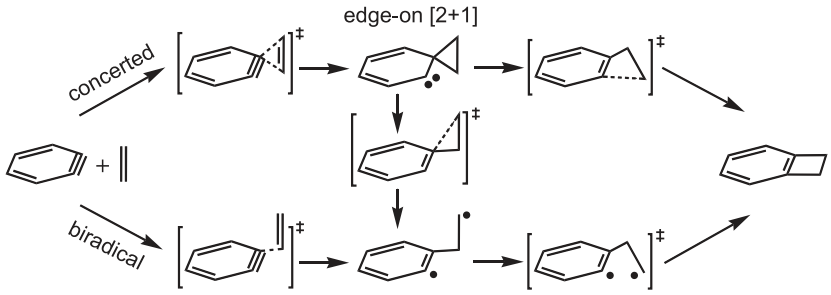

Scheme 1: Benzocyclobutene forming ″concerted″ and biradical reaction pathway for the reaction *o*-benzyne + ethene.

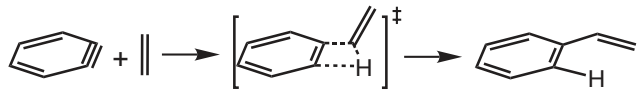

Scheme 2: Styrene forming concerted reaction pathway for the reaction *o*-benzyne + ethene.

Scheme 3: *Ene*-type [4+2] cycloaddition in presence of an allylic hydrogen in the alkene component. Formation of the open chain, terminal alkene product for the reaction *o*-benzyne + propene.

Table 1: Comparison of the reactivity of *o*-C_6H_4 towards C_2H_2, C_2H_4, C_3H_6, and *trans*-C_4H_8.

reactant	$[o\text{-}C_6H_4]/[o\text{-}C_6H_4]_0$ [a]	E_0 [b] (kJ/mol)	main product	k(1475 K) ($cm^3mol^{-1}s^{-1}$)	A [c] ($cm^3mol^{-1}s^{-1}$)
C_2H_2	0.98	63	benzocyclobutadiene	2.2×10^{11}	3.7×10^{13}
C_2H_4	0.83	43	benzocyclobutene	2.1×10^{12}	7.0×10^{13}
C_3H_6	0.72	20	allylbenzene	3.6×10^{12}	1.8×10^{13}
trans-C_4H_8	0.35			1.2×10^{13}	

a: Measured at 10 vol-% reactant concentration.
b: Zero-point energy barrier of main product pathway (B3LYP/6-311+G(d,p)).
c: Calculated preexponential Arrhenius factor assuming E_a=E_0.

The Products of the Reactions of *o*-Benzyne with Ethene, Propene, and Acetylene: A Combined Mass Spectrometric and Quantum Chemical Study

G. Friedrichs, E. Goos, J. Gripp, H. Nicken, J.-B. Schönborn, H. Vogel, and F. Temps

Supplement

Tables of energies and structures of reactants, transition states, intermediates, and products. Energies are given in Hartree (E_h), and Cartesian coordinates in Ångström (Å).

REACTANTS

C_6H_4 (*o*-Benzyne)

B3LYP/6-311+G(d,p)

Zero-point correction ZP = 0.074890

Electronic energy (including ZP) E = -230.897795

C	0.000000	0.702713	1.056666
C	0.000000	-0.702713	1.056666
C	0.000000	-1.459308	-0.133940
C	0.000000	-0.622194	-1.234437
C	0.000000	0.622194	-1.234437
C	0.000000	1.459308	-0.133940
H	0.000000	1.227056	2.007018
H	0.000000	-1.227056	2.007018
H	0.000000	-2.541411	-0.136755
H	0.000000	2.541411	-0.136755

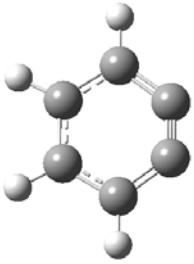

C_2H_4 (Ethene)

B3LYP/6-311+G(d,p)

Zero-point correction ZP = 0.050782

Electronic energy (including ZP) E = -78.564730

C	0.000000	0.000000	0.664389
H	0.000000	0.922841	1.235170
H	0.000000	-0.922841	1.235170
C	0.000000	0.000000	-0.664389
H	0.000000	-0.922841	-1.235170
H	0.000000	0.922841	-1.235170

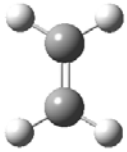

C_3H_6 (Propene)

B3LYP/6-311+G(d,p)

Zero-point correction ZP = 0.079286

Electronic energy (including ZP) E = -117.866302

C	0.000000	0.472778	0.000000
H	0.277272	1.525954	0.000000
C	-1.291777	0.151513	0.000000
H	-2.066396	0.910172	0.000000
H	-1.620530	-0.883905	0.000000
C	1.137744	-0.505325	0.000000
H	1.777013	-0.364085	0.878717
H	0.779822	-1.537845	0.000000
H	1.777013	-0.364085	-0.878717

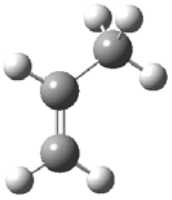

C_2H_2 (Acetylene)

B3LYP/6-311+G(d,p)

Zero-point correction ZP = 0.027031

Electronic energy (including ZP) E = -77.329615

C	0.000000	0.000000	0.599684
H	0.000000	0.000000	1.662817
C	0.000000	0.000000	-0.599684
H	0.000000	0.000000	-1.662817

INTERMEDIATES & TRANSITION STATES

Intermediates (*o*-C_6H_4 + C_2H_4)

C_8H_8 'edge-on' B3LYP/6-311+G(d,p)

Zero-point correction ZP = 0.131004

Electronic energy (including ZP) E = -309.461894

C	0.082146	1.219990	-0.000030
C	1.437107	-1.243317	0.000016
C	2.121194	-0.041855	-0.000011
C	1.444844	1.210971	0.000007
H	-0.467183	2.158342	-0.000030
H	2.023559	-2.159996	0.000004
H	3.209258	-0.037029	-0.000031
H	2.011678	2.134576	0.000085
H	-2.265707	0.875940	-1.258181
H	-2.234078	-0.965493	-1.247480
C	0.015948	-1.340608	0.000070
C	-0.621969	-0.045960	-0.000081
C	-2.054420	-0.039444	-0.720647
C	-2.054503	-0.039336	0.720669
H	-2.265459	0.876266	1.257939
H	-2.234155	-0.965245	1.247742

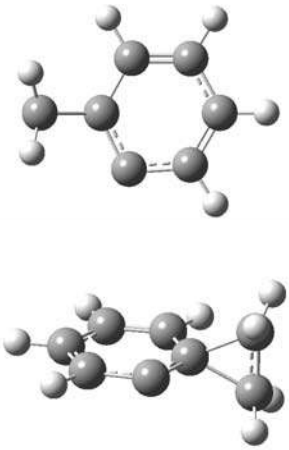

C_8H_8 'biradical' B3LYP/6-311+G(d,p)

Zero-point correction ZP = 0.128249

Electronic energy (including ZP) E = -309.473949

C	0.554179	0.215330	-0.001820
C	-0.457560	1.065677	0.376957
C	0.266063	-1.154248	0.138510
C	-0.966661	-1.580923	0.631755
C	-1.945507	-0.658104	1.001830
C	-1.687275	0.714981	0.878518
H	1.022382	-1.885046	-0.134834
H	-1.162740	-2.642414	0.733263
H	-2.902455	-0.995755	1.385331
H	-2.429298	1.452230	1.165011
C	1.864441	0.820568	-2.053500
C	1.894232	0.700150	-0.565306
H	1.386941	1.672863	-2.521674
H	2.127379	-0.020884	-2.683096
H	2.126716	1.667060	-0.110388
H	2.672644	-0.003375	-0.255495

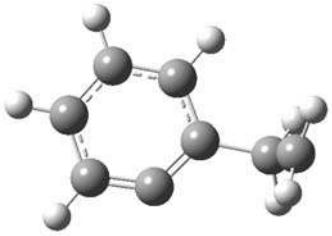

Transition States (*o*-C_6H_4 + C_2H_4)

$C_8H_8^{\#}$ 'edge-on #1'

B3LYP/6-311+G(d,p)

Zero-point correction ZP = 0.127771

Electronic energy (including ZP) E = -309.441414

C	0.410320	-0.131126	-0.140110
C	-0.111703	1.162546	-0.095697
C	-1.499286	1.220341	0.019934
C	-2.257196	0.039796	0.095441
C	-1.643596	-1.217408	0.053736
C	-0.245095	-1.254798	0.010034
H	0.487382	2.061141	-0.208788
H	-1.995957	2.184330	0.036008
H	-3.334901	0.109528	0.215301
H	-2.251087	-2.115533	0.122513
C	2.657770	0.054652	0.653335
H	2.770261	1.065701	1.026057
H	2.789332	-0.749966	1.365968
C	2.191914	-0.197501	-0.623818
H	2.270010	-1.199539	-1.021231
H	2.246187	0.585326	-1.372956

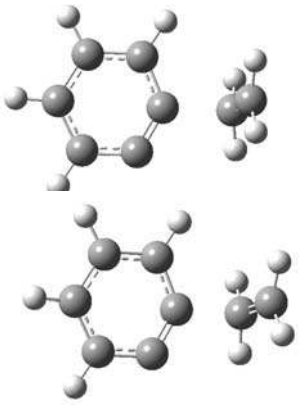

$C_8H_8^{\#}$ 'edge-on #2'

B3LYP/6-311+G(d,p)

Zero-point correction ZP = 0.130255

Electronic energy (including ZP) E = -309.449784

C	-0.214732	1.319794	-0.011051
C	-1.224342	-1.303126	-0.068195
C	-2.069638	-0.227099	0.067672
C	-1.556101	1.103265	0.112993
H	0.206703	2.314339	0.102613
H	-1.641251	-2.305697	-0.006344
H	-3.142073	-0.374018	0.167227
H	-2.235047	1.932623	0.279530
H	1.644526	0.038816	1.734328
H	2.051468	-1.519050	0.839080
C	0.158375	-1.150100	-0.419998
C	0.626260	0.194467	-0.339391
C	1.816515	-0.469664	0.793896
C	2.130170	0.330484	-0.410755
H	2.507782	1.336115	-0.248497
H	2.608860	-0.211250	-1.218968

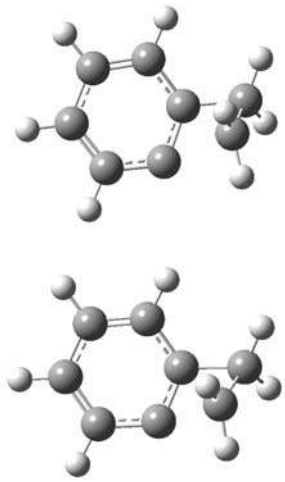

$C_8H_8^{\#}$ 'H-transfer #'

B3LYP/6-311+G(d,p)

Zero-point correction ZP = 0.126556

Electronic energy (including ZP) E = -309.430648

C	-0.041677	-0.014536	0.028818
C	0.033219	0.027441	2.865491
C	1.217563	0.025872	2.109353
C	1.177044	0.003922	0.712405
H	-0.056193	-0.027558	-1.056653
H	0.072423	0.039655	3.949767
H	2.175811	0.032703	2.620775
H	2.105732	0.000279	0.152493
H	-4.126850	1.228383	-0.750014
H	-2.360512	1.620594	-1.136747
C	-1.145818	-0.005248	2.148407
C	-1.216990	-0.010131	0.790828
C	-3.077153	0.988513	-0.626464
C	-2.661601	-0.010566	0.310709
H	-3.255253	0.069608	1.277043
H	-2.922417	-1.038251	0.006774

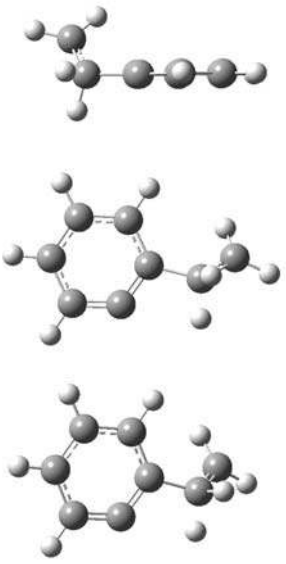

$C_8H_8^{\#}$ 'biradical #1'

B3LYP/6-311+G(d,p)

Zero-point correction ZP = 0.126474

Electronic energy (including ZP) E = -309.446193

C	0.309795	0.244988	0.034933
C	-0.584544	1.058674	0.480493
C	0.137578	-1.125086	-0.105179
C	-1.111950	-1.592065	0.323444
C	-2.080234	-0.716188	0.835657
C	-1.834310	0.662253	0.936835
H	0.895350	-1.796797	-0.495590
H	-1.332328	-2.652375	0.258069
H	-3.042940	-1.109571	1.147661
H	-2.589243	1.338587	1.322641
C	2.381746	0.695787	-1.748857
C	2.208178	0.921065	-0.408402
H	2.110386	1.443593	-2.484785
H	2.694007	-0.271247	-2.126632
H	2.042778	1.930368	-0.056174
H	2.661411	0.251002	0.314369

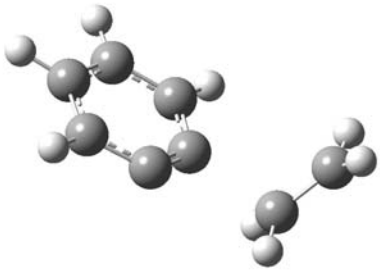

$C_8H_8^{\#}$ 'biradical #2'

B3LYP/6-311+G(d,p)

Zero-point correction ZP = 0.127743

Electronic energy (including ZP) E = -309.474517

C	-0.123192	0.542512	-0.201399
C	-1.108699	-0.385318	-0.455064
C	0.745053	0.212081	0.855969
C	0.586786	-0.972877	1.572885
C	-0.438478	-1.866473	1.258267
C	-1.319989	-1.569723	0.209877
H	1.548190	0.897649	1.111074
H	1.267570	-1.200796	2.385315
H	-0.557182	-2.786611	1.820496
H	-2.125295	-2.246430	-0.053954
C	1.164294	1.752165	-1.996102
C	0.048730	1.817432	-1.004554
H	1.467326	0.805312	-2.424870
H	1.588032	2.662419	-2.403493
H	-0.901397	2.036418	-1.516459
H	0.209296	2.660957	-0.321131

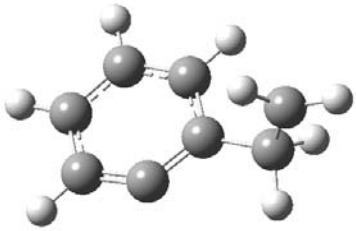

$C_8H_8^{\#}$ 'biradical ↔ edge-on #'

B3LYP/6-311+G(d,p)

Zero-point correction ZP = 0.128344

Electronic energy (including ZP) E = -309.451220

C	0.627859	0.034928	0.165294
C	-0.061136	1.254520	0.156370
C	-0.100685	-1.193970	0.174531
C	-1.479360	-1.153142	0.125930
C	-2.156918	0.079991	0.149867
C	-1.440895	1.276431	0.283653
H	0.420663	-2.141253	0.286596
H	-2.047596	-2.076740	0.114204
H	-3.239491	0.098953	0.067337
H	-1.978544	2.213227	0.401932
C	2.163875	0.006374	0.284007
C	2.066198	0.013943	-1.165836
H	1.989806	0.948069	-1.702969
H	2.018510	-0.908890	-1.726854
H	2.533546	-0.907011	0.743406
H	2.565304	0.898740	0.751086

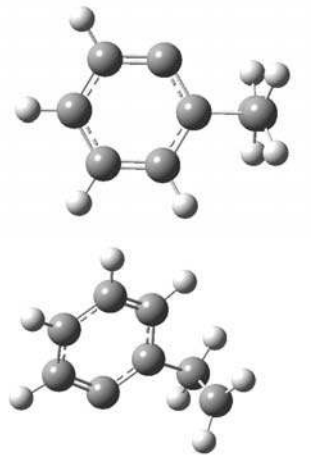

Intermediates (*o*-C_6H_4 + C_3H_6)

C_9H_{10} 'edge-on (cis)'

B3LYP/6-311+G(d,p)

Zero-point correction ZP = 0.158674

Electronic energy (including ZP) E = -348.761214

C	0.680336	-1.261513	-0.181975
C	1.559478	1.365358	0.250485
C	2.426521	0.380030	-0.188096
C	1.991225	-0.955564	-0.405714
H	0.319865	-2.279969	-0.309031
H	1.969104	2.359424	0.420555
H	3.472052	0.618056	-0.372907
H	2.695360	-1.712554	-0.730817
H	-1.397637	-1.705985	1.457019
H	-1.754602	0.055906	1.836620
C	0.167811	1.153798	0.456659
C	-0.221416	-0.209843	0.230535
C	-1.485700	-0.687945	1.099158
C	-1.771614	-0.427162	-0.286622
H	-1.803051	-1.291492	-0.941770
C	-2.552272	0.770412	-0.760089
H	-2.283459	1.034523	-1.785471
H	-3.620452	0.525304	-0.738988
H	-2.363408	1.631352	-0.121259

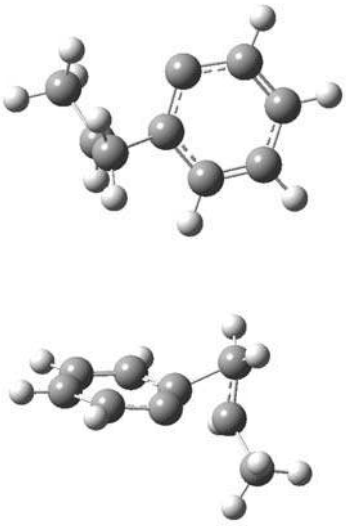

C_9H_{10} 'edge-on (trans)'

B3LYP/6-311+G(d,p)

Zero-point correction ZP = 0.158876

Electronic energy (including ZP) E = -348.760641

C	0.266839	1.045537	0.478222
C	1.968964	-1.007129	-0.403468
C	2.429351	0.285969	-0.235680
C	1.577182	1.328123	0.221854
H	-0.394659	1.821369	0.852358
C	-0.209703	-0.300652	0.258652
C	0.616381	-1.394318	-0.185572
H	1.972103	2.326037	0.372936
H	3.469179	0.526009	-0.447892
H	2.682171	-1.761465	-0.730163
C	-1.747907	-0.460918	-0.311183
C	-1.507887	-0.737082	1.080843
H	-1.740752	-1.320929	-0.969320
H	-1.436708	-1.760998	1.419130
H	-1.812332	-0.005307	1.820233
C	-2.495910	0.746852	-0.814535
H	-2.089770	1.101679	-1.764478
H	-3.539528	0.461182	-0.984574
H	-2.493560	1.574128	-0.103031

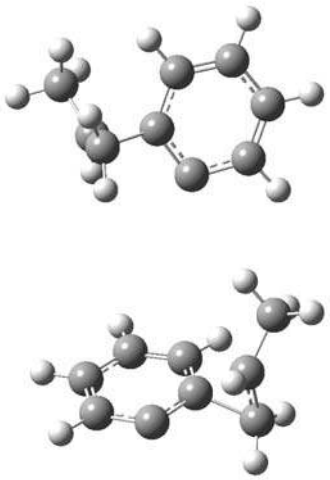

C_9H_{10} 'biradical' B3LYP/6-311+G(d,p)

Zero-point correction ZP = 0.156222

Electronic energy (including ZP) E = -348.772941

C	0.085880	-0.213736	0.304861
C	0.970192	-1.239782	0.056066
C	0.648279	1.076512	0.268310
C	2.002540	1.262630	-0.004239
C	2.838782	0.172013	-0.249946
C	2.312321	-1.126292	-0.220152
H	0.009686	1.934799	0.456258
H	2.410523	2.267000	-0.023322
H	3.892022	0.323752	-0.461094
H	2.940711	-1.990506	-0.405451
C	-1.384892	-0.437790	0.587789
H	-1.555424	-1.519451	0.715737
H	-1.638806	0.005139	1.562943
C	-2.300702	0.110816	-0.461459
H	-1.900750	0.290228	-1.453466
C	-3.775927	0.120354	-0.251503
H	-4.289234	0.724184	-1.003709
H	-4.205952	-0.894139	-0.305224
H	-4.041621	0.510646	0.738975

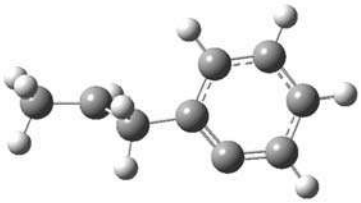

Transition States (*o*-C_6H_4 + C_3H_6)

$C_9H_{10}^{\#}$ 'edge-on #1, trans' B3LYP/6-311+G(d,p)

Zero-point correction ZP = 0.155760

Electronic energy (including ZP) E = -348.746395

C	0.389601	0.989997	0.450603
C	2.237662	-0.985710	-0.389054
C	2.628713	0.350681	-0.248524
C	1.715126	1.328727	0.173187
H	-0.311035	1.729634	0.824883
C	0.089391	-0.360988	0.279762
C	0.891497	-1.293693	-0.161907
H	2.041973	2.354973	0.302681
H	3.649353	0.642161	-0.480820
H	2.962870	-1.728719	-0.709569
C	-2.324390	-0.522877	-0.283300
C	-1.622417	-0.816435	0.872952
H	-2.346109	-1.278100	-1.064587
H	-1.452736	-1.853219	1.124673
H	-1.736442	-0.160277	1.731225
C	-2.926112	0.794569	-0.617334
H	-2.412742	1.258926	-1.469314
H	-3.969244	0.660797	-0.929952
H	-2.905514	1.488836	0.224745

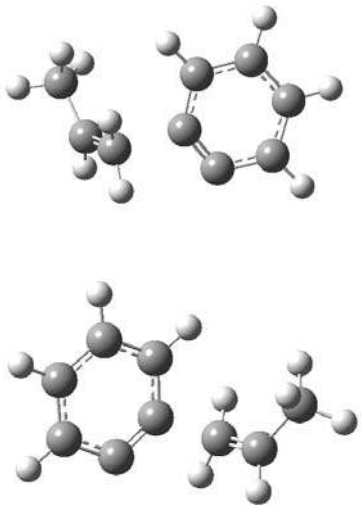

C_9H_{10}[#] 'edge-on #2, trans' B3LYP/6-311+G(d,p)

Zero-point correction ZP = 0.157980

Electronic energy (including ZP) E = -348.751545

C	-0.482960	1.271685	-0.338266
C	-1.540665	-1.279568	0.159509
C	-2.304439	-0.150686	0.364375
C	-1.762299	1.143836	0.128624
H	-0.026437	2.250816	-0.452951
C	0.225315	0.079841	-0.714264
C	-0.279891	-1.238180	-0.514731
H	-2.359528	2.022923	0.345800
H	-3.325293	-0.230221	0.729851
H	-1.955163	-2.245422	0.440595
C	1.731998	-0.515651	0.141782
C	1.667695	0.141087	-1.179808
H	1.882729	-1.582903	0.153209
H	1.903834	-0.489181	-2.031358
H	2.080492	1.145644	-1.238412
C	2.000251	0.213324	1.422368
H	1.401836	-0.187755	2.243514
H	3.054941	0.061504	1.685892
H	1.813336	1.285630	1.348292

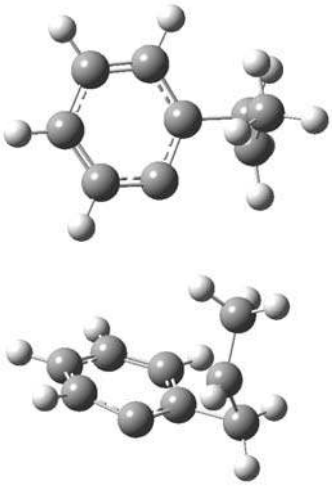

C_9H_{10}[#] 'ene #' B3LYP/6-311+G(d,p)

Zero-point correction ZP = 0.155357

Electronic energy (including ZP) E = -348.756465

C	1.073303	-1.352714	-0.049854
C	1.581116	1.468919	0.075792
C	2.625992	0.541506	-0.061985
C	2.379258	-0.838526	-0.122432
H	0.873347	-2.416931	-0.086347
H	1.786323	2.533291	0.123233
H	3.649564	0.897805	-0.127204
H	3.211312	-1.527359	-0.226349
H	-1.794875	-2.226078	0.057190
H	-1.843288	-1.021552	1.450294
C	0.301463	0.913510	0.131274
C	0.133119	-0.349725	0.082645
C	-1.961400	-1.207785	0.388937
C	-2.579584	-0.306011	-0.414208
H	-2.764088	-0.578899	-1.450405
C	-2.736174	1.103037	-0.035594
H	-3.377836	1.675946	-0.705158
H	-3.050232	1.242076	1.001081
H	-1.686152	1.530289	-0.081484

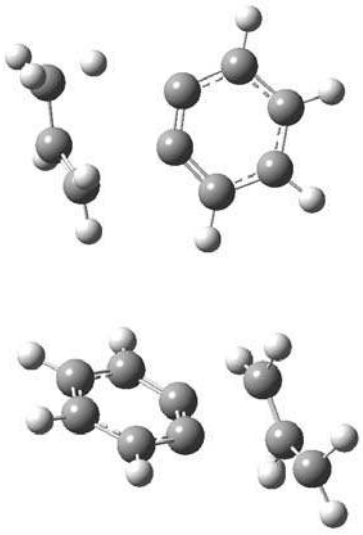

$C_9H_{10}^{\#}$ 'H-transfer #, cis'

B3LYP/6-311+G(d,p)

Zero-point correction ZP = 0.154968

Electronic energy (including ZP) E = -348.736717

C	-0.373730	0.936736	0.569178
C	-2.166679	-0.966228	-0.484975
C	-2.579607	0.355111	-0.257247
C	-1.689932	1.293890	0.273255
H	0.308426	1.678003	0.980049
H	-2.872402	-1.694960	-0.872965
H	-3.604290	0.644501	-0.473783
H	-2.026895	2.307883	0.459104
H	3.457906	-1.021925	-0.153181
C	-0.859480	-1.292156	-0.162740
C	0.032554	-0.383155	0.319947
C	2.583872	-0.384603	-0.052008
C	1.422128	-0.972572	0.575525
H	1.334755	-2.048896	0.273190
H	1.552051	-1.058413	1.668048
C	2.630572	0.951346	-0.675959
H	1.777128	1.086176	-1.357090
H	2.515670	1.757080	0.067777
H	3.559460	1.120336	-1.220996

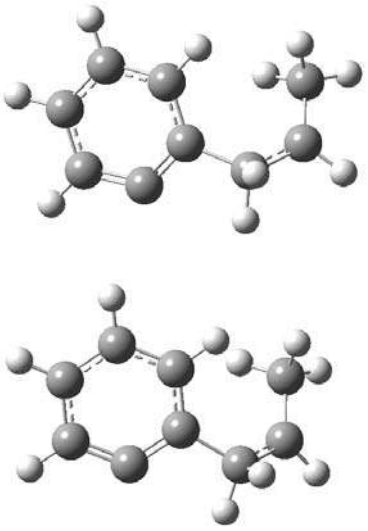

$C_9H_{10}^{\#}$ 'H-transfer #, trans'

B3LYP/6-311+G(d,p)

Zero-point correction ZP = 0.154499

Electronic energy (including ZP) E = -348.737992

C	-0.787727	1.198317	0.221537
C	-2.123006	-1.263087	-0.187084
C	-2.813811	-0.044103	-0.280029
C	-2.153096	1.169952	-0.074737
H	-0.290321	2.149168	0.388807
H	-2.651192	-2.199784	-0.337335
H	-3.876353	-0.046662	-0.506482
H	-2.708096	2.099377	-0.141357
H	2.017772	1.132470	-0.946571
C	-0.770877	-1.204534	0.104317
C	-0.107758	-0.023562	0.297171
C	2.344380	0.374585	-0.239768
C	1.361343	-0.263315	0.590715
H	1.440322	-1.396996	0.488821
H	1.557165	-0.139014	1.667922
C	3.743079	-0.096583	-0.338992
H	3.866039	-0.752085	-1.218823
H	4.435972	0.737734	-0.491488
H	4.053537	-0.670234	0.537716

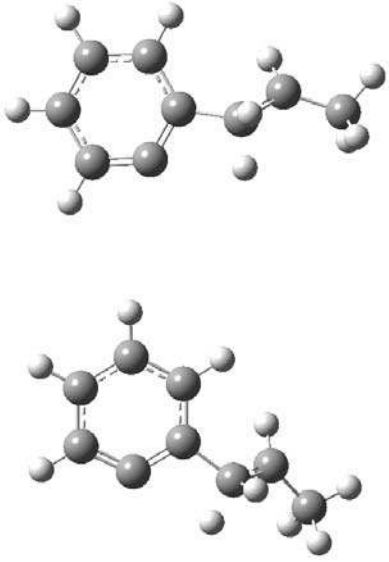

$C_9H_{10}^{\#}$ (biradical #1, trans)

B3LYP/6-311+G(d,p)

Zero-point correction ZP = 0.154736

Electronic energy (including ZP) E =-348.745219

C	0.176337	-0.371298	0.246001
C	1.026870	-1.266621	-0.127694
C	0.444764	0.981163	0.410797
C	1.777121	1.333295	0.157175
C	2.721416	0.371254	-0.228582
C	2.366397	-0.978809	-0.368238
H	-0.282731	1.719252	0.731140
H	2.082230	2.368490	0.269350
H	3.743847	0.678683	-0.427048
H	3.103502	-1.718692	-0.662799
C	-1.738097	-0.900127	0.769414
H	-1.511699	-1.946621	0.918160
H	-1.740214	-0.295413	1.671493
C	-2.516985	-0.526903	-0.296835
H	-2.649820	-1.238028	-1.108688
C	-3.090823	0.833965	-0.505861
H	-2.607403	1.340481	-1.351576
H	-4.156286	0.770629	-0.755843
H	-2.983442	1.465712	0.378742

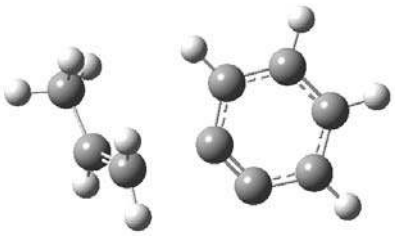

$C_9H_{10}^{\#}$ 'biradical ↔ edge-on'

B3LYP/6-311+G(d,p)

Zero-point correction ZP = 0.157323

Electronic energy (including ZP) E = -348.758458

C	0.146646	-0.293252	0.355094
C	-0.186822	1.051679	0.505695
C	-0.755518	-1.282647	-0.122907
C	-2.039849	-0.892382	-0.442788
C	-2.429511	0.443673	-0.228906
C	-1.542095	1.366582	0.326187
H	-0.472406	-2.332030	-0.165630
H	-2.754762	-1.614778	-0.820209
H	-3.430719	0.754818	-0.516006
H	-1.900326	2.373760	0.527970
C	1.540585	-0.822111	0.904845
C	1.958763	-0.429359	-0.406441
H	1.832856	-1.135667	-1.217735
H	1.483391	-1.882359	1.130366
H	1.896742	-0.223045	1.735406
C	2.534636	0.904516	-0.659586
H	3.483925	1.029550	-0.126768
H	2.677629	1.112212	-1.720027
H	1.822666	1.637355	-0.214526

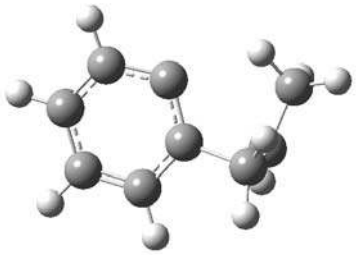

Intermediates (*o*-C_6H_4 + C_2H_2)

C_8H_6 'addition complex' B3LYP/6-311+G(d,p)

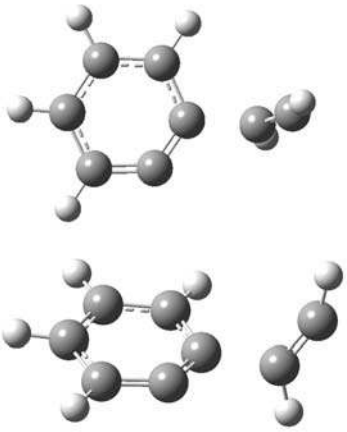

Zero-point correction ZP = 0.103794

Electronic energy (including ZP) E = -308.209283

C	0	-0.031001	1.154764	-0.121477
C	0	-1.576776	-1.219756	0.075924
C	0	-2.184874	0.045115	0.111210
C	0	-1.418385	1.213486	0.013006
H	0	0.567297	2.051853	-0.244666
H	0	-2.170901	-2.122653	0.170624
H	0	-3.260272	0.117109	0.246791
H	0	-1.909974	2.179947	0.033576
H	0	3.146754	0.263889	1.522530
C	0	-0.196354	-1.206205	-0.004150
C	0	0.538171	-0.128095	-0.153608
C	0	2.931054	0.036272	0.498661
C	0	2.151377	-0.226338	-0.459952
H	0	2.347819	-0.505598	-1.486544

C_8H_6 'edge-on' B3LYP/6-311+G(d,p)

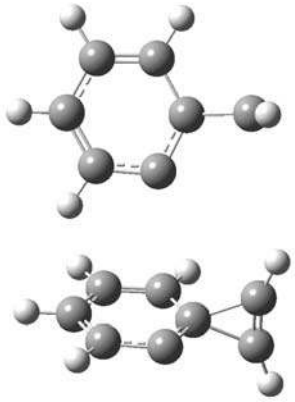

Zero-point correction ZP = 0.105034

Electronic energy (including ZP) E = -308.210814

C	-0.001031	1.208274	0.000148
C	-1.386070	-1.234179	-0.000180
C	-2.057437	-0.024273	-0.000043
C	-1.365937	1.218431	0.000123
H	0.568132	2.133444	0.000273
H	-1.986011	-2.142565	-0.000304
H	-3.145510	-0.006975	-0.000061
H	-1.919975	2.149978	0.000227
C	0.035280	-1.353638	-0.000167
C	0.684490	-0.069389	0.000004
C	2.162015	-0.039203	0.627638
C	2.162042	-0.039045	-0.627559
H	2.541662	-0.067669	-1.629400
H	2.541590	-0.068078	1.629489

Transition States (*o*-C_6H_4 + C_2H_2)

$C_8H_6^{\#}$ 'addition complex #' B3LYP/6-311+G(d,p)

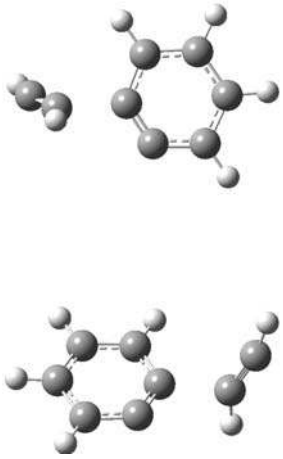

Zero-point correction ZP = 0.102802

Electronic energy (including ZP) E = -308.208661

C	0.038906	1.154094	0.118242
C	1.632781	-1.212176	-0.096690
C	2.216265	0.065120	-0.094363
C	1.433636	1.224257	0.011063
H	-0.577722	2.039614	0.221961
H	2.244274	-2.103050	-0.193016
H	3.293696	0.158602	-0.195473
H	1.914914	2.196466	0.012184
C	0.245847	-1.216164	-0.015012
C	-0.453530	-0.146997	0.117822
C	-3.005247	0.057902	-0.493084
C	-2.305321	-0.264812	0.471181
H	-2.329726	-0.592395	1.492348
H	-3.331686	0.345439	-1.466494

$C_8H_6^{\#}$ 'edge-on #1' B3LYP/6-311+G(d,p)

Zero-point correction ZP = 0.103513

Electronic energy (including ZP) E = -308.204034

C	-0.008896	1.187773	-0.110156
C	-1.445253	-1.229916	-0.002147
C	-2.098576	-0.001190	0.088142
C	-1.383605	1.212732	0.021682
H	0.561974	2.098346	-0.260901
H	-2.041559	-2.139487	0.011058
H	-3.176020	0.031323	0.229675
H	-1.913463	2.158202	0.046829
H	2.578260	0.123482	1.697751
C	-0.038760	-1.294806	0.019379
C	0.598890	-0.093586	-0.131346
C	2.478592	0.029494	0.640616
C	2.137655	-0.142281	-0.550867
H	2.503779	-0.288246	-1.552998

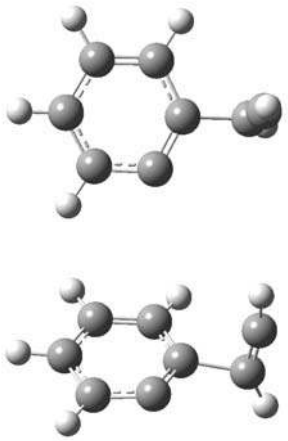

$C_8H_6^{\#}$ 'edge-on #2' B3LYP/6-311+G(d,p)

Zero-point correction ZP = 0.104652

Electronic energy (including ZP) E = -308.203301

C	-0.089275	1.283351	0.068285
C	-1.242095	-1.280050	-0.027076
C	-2.030450	-0.149138	0.020676
C	-1.447881	1.150728	0.090399
H	0.387862	2.240589	0.254041
H	-1.715786	-2.254707	0.060593
H	-3.114095	-0.232608	0.051644
H	-2.087166	2.015963	0.227163
C	0.151963	-1.212148	-0.335849
C	0.692268	0.107565	-0.246575
C	1.998483	-0.445886	0.636558
C	2.213721	0.263269	-0.398788
H	2.883307	0.838607	-1.010214
H	2.161779	-0.874833	1.606261

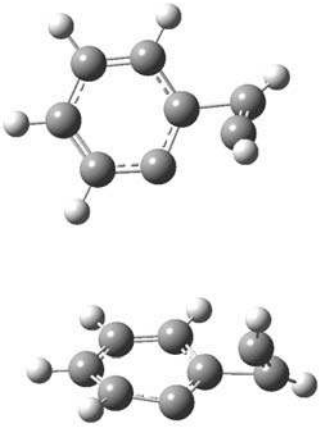

C_8H_6 'H-transfer #' B3LYP/6-311+G(d,p)

Zero-point correction ZP = 0.101689

Electronic energy (including ZP) E = -308.198734

C	0.542790	-0.047746	0.002250
C	-0.157922	-1.302487	-0.018204
C	-1.545695	-1.204954	-0.000005
C	-2.196356	0.034375	0.002402
C	-1.481836	1.233937	-0.002396
C	-0.093423	1.202015	0.000744
H	-2.158027	-2.103939	-0.003545
H	-3.281775	0.055377	0.005888
H	-2.008257	2.181504	-0.000485
H	0.477363	2.122488	0.015386
C	1.960285	-0.307973	0.022251
C	3.119294	0.203452	-0.020792
H	1.911999	-1.475891	0.068727
H	4.175881	0.356754	-0.003465

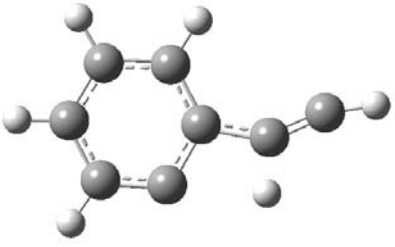

Remark: TS did not fully converge, but only 1 imaginary frequency. See text.

PRODUCTS

o-C_6H_4 + C_2H_4

C_8H_8 Benzocyclobutene

B3LYP/6-311+G(d,p)

Zero-point correction ZP = 0.133856

Electronic energy (including ZP) E = -309.574708

C	0.452878	-0.696832	0.000000
C	0.452878	0.696832	0.000000
C	-0.718896	-1.436783	0.000000
C	-1.912755	-0.700160	0.000000
C	-1.912755	0.700160	0.000000
C	-0.718896	1.436783	0.000000
H	-0.734941	-2.521438	0.000000
H	-2.862332	-1.224507	0.000000
H	-2.862332	1.224507	0.000000
H	-0.734941	2.521438	0.000000
C	1.972599	0.791332	0.000000
C	1.972599	-0.791332	0.000000
H	2.417854	1.246490	0.888446
H	2.417854	1.246490	-0.888446
H	2.417854	-1.246490	0.888446
H	2.417854	-1.246490	-0.888446

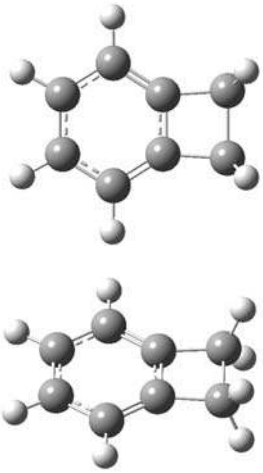

C_8H_8 Styrene

B3LYP/6-311+G(d,p)

Zero-point correction ZP = 0.132759

Electronic energy (including ZP) E = -309.598034

C	-0.000293	0.559108	0.002427
C	-1.006537	-0.421491	-0.013851
C	1.335703	0.130242	0.009022
C	1.660082	-1.224294	-0.002603
C	0.650057	-2.182744	-0.020008
C	-0.685229	-1.773229	-0.025180
H	2.127898	0.871924	0.022582
H	2.700551	-1.529536	0.002216
H	0.897061	-3.238277	-0.028615
H	-1.478007	-2.513084	-0.037163
C	-1.477277	2.602595	-0.019180
C	-0.282737	2.003697	0.013145
H	-2.410489	2.052171	-0.060062
H	-1.555904	3.682951	-0.006851
H	-2.049317	-0.126231	-0.015883
H	0.602392	2.635258	0.050004

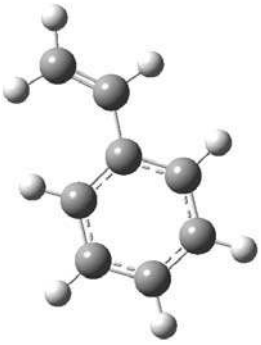

o-C_6H_4 + C_3H_6

C_9H_{10} Allylbenzene B3LYP/6-311+G(d,p)

Zero-point correction ZP = 0.160948

Electronic energy (including ZP) E = -348.890052

C	0.998687	-1.276172	-0.008505
C	0.003433	-0.328305	-0.261559
C	0.360683	1.025423	-0.274530
C	1.676971	1.418563	-0.047596
C	2.661996	0.462532	0.202371
C	2.318537	-0.886835	0.222169
H	0.740375	-2.330466	0.005219
H	-0.401109	1.775661	-0.459639
H	1.935023	2.471858	-0.064439
H	3.686822	0.768318	0.380447
H	3.075882	-1.638457	0.416250
C	-1.433813	-0.750402	-0.521513
H	-1.740101	-0.429868	-1.523481
H	-1.481286	-1.845483	-0.514990
C	-2.408539	-0.208663	0.492393
H	-2.198877	-0.463192	1.529769
C	-3.471777	0.539806	0.207119
H	-3.713320	0.820283	-0.814082
H	-4.140474	0.895663	0.982855

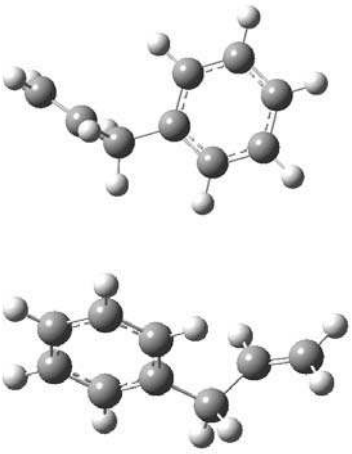

C_9H_{10} E-Phenylpropene B3LYP/6-311+G(d,p)

Zero-point correction ZP = 0.160665

Electronic energy (including ZP) E = -348.899545

C	-0.058378	-0.205421	-0.000166
C	-0.583845	1.098447	-0.000229
C	-1.956138	1.317081	-0.000060
C	-2.845310	0.240195	0.000156
C	-2.342964	-1.058583	0.000175
C	-0.967133	-1.275569	0.000004
H	0.084912	1.951296	-0.000465
H	-2.336613	2.332728	-0.000124
H	-3.915265	0.414407	0.000276
H	-3.021232	-1.904759	0.000317
H	-0.585002	-2.291468	0.000019
C	1.383332	-0.499558	-0.000312
H	1.628315	-1.560720	-0.000915
C	2.397763	0.373650	0.000291
H	2.189643	1.441427	0.001011
C	3.847725	-0.005861	0.000098
H	4.362424	0.401171	-0.877958
H	4.362378	0.400003	0.878721
H	3.980130	-1.090373	-0.000626

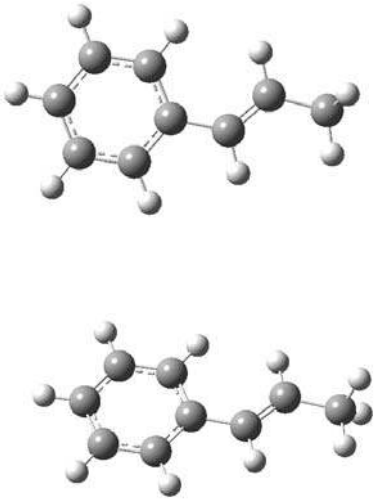

C_9H_{10} Z-Phenylpropene B3LYP/6-311+G(d,p)

Zero-point correction ZP = 0.161078

Electronic energy (including ZP) E = -348.895067

C	0.054038	0.069832	0.074635
C	1.454281	0.173290	0.103696
C	2.082683	1.413433	0.017107
C	1.328881	2.579296	-0.105875
C	-0.062181	2.493095	-0.157017
C	-0.688360	1.253478	-0.076598
H	2.056996	-0.724161	0.162421
H	3.165766	1.467451	0.034823
H	1.820042	3.543388	-0.173832
H	-0.659069	3.392157	-0.264129
H	-1.771096	1.194724	-0.121469
C	-0.663742	-1.216652	0.152629
H	-1.582065	-1.252757	-0.429684
C	-0.358716	-2.311765	0.864694
H	-1.036218	-3.157017	0.765477
C	0.779171	-2.518376	1.822086
H	1.230253	-1.578989	2.144121
H	0.429167	-3.052922	2.710597
H	1.569068	-3.136956	1.378238

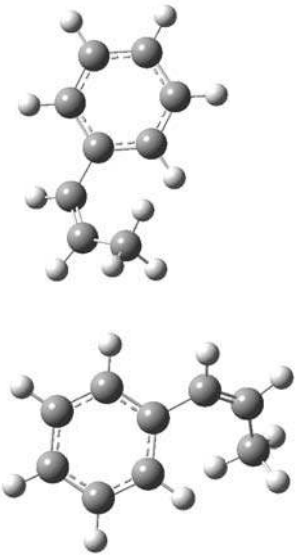

C_9H_{10} 1-Methylbenzocyclobutene B3LYP/6-311+G(d,p)

Zero-point correction ZP = 0.161704

Electronic energy (including ZP) E = -348.873631

C	-1.454742	1.294014	0.186350
C	-0.724152	-1.454199	-0.221769
C	-2.053176	-1.073261	0.015853
C	-2.409428	0.266520	0.213379
H	-1.746183	2.327331	0.341742
C	-0.145198	0.902956	-0.043963
C	0.208574	-0.428844	-0.245685
H	-3.450908	0.511228	0.392538
H	-2.827976	-1.831818	0.046649
H	-0.465214	-2.496323	-0.376528
C	1.690683	-0.109492	-0.435018
C	1.283192	1.405311	-0.191541
H	2.032106	-0.277495	-1.462124
H	1.470363	2.076432	-1.034310
H	1.720952	1.842541	0.710647
C	2.681017	-0.721687	0.550854
H	2.766238	-1.802367	0.402677
H	3.677815	-0.287677	0.424664
H	2.362189	-0.549754	1.583294

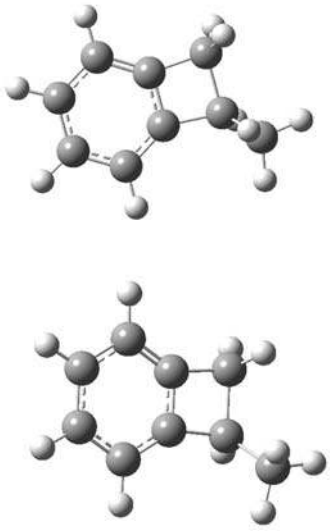

o-C_6H_4 + C_2H_2

C_8H_6 Phenylacetylene B3LYP/6-311+G(d,p)

Zero-point correction ZP =0.109174

Electronic energy (including ZP) E =-308.368075

C	-0.000155	0.593899	0.000000
C	-1.210678	-0.119782	0.000000
C	-1.205871	-1.510456	0.000000
C	0.000848	-2.209777	0.000000
C	1.207064	-1.509602	0.000000
C	1.210862	-0.118923	0.000000
H	-2.146394	-2.049630	0.000000
H	0.001240	-3.293801	0.000000
H	2.147968	-2.048108	0.000000
H	2.146345	0.427329	0.000000
C	-0.000763	2.021952	0.000000
C	-0.001656	3.226993	0.000000
H	-2.146561	0.425785	0.000000
H	-0.002457	4.289346	0.000000

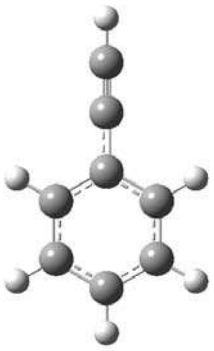

C_8H_6 Benzocyclobutadiene B3LYP/6-311+G(d,p)

Zero-point correction ZP = 0.109770

Electronic energy (including ZP) E = -308.328257

C	-0.000001	0.711200	0.522254
C	0.000001	-0.711200	0.522254
C	0.000002	-1.443153	-0.623477
C	0.000001	-0.688396	-1.844026
C	-0.000001	0.688396	-1.844026
C	-0.000002	1.443153	-0.623477
H	0.000003	-2.526936	-0.644274
H	0.000002	-1.220297	-2.788776
H	-0.000002	1.220297	-2.788776
H	-0.000003	2.526936	-0.644274
C	0.000001	0.675028	2.046570
C	-0.000001	-0.675028	2.046570
H	0.000000	1.425452	2.824942
H	0.000000	-1.425452	2.824942